Accepted Manuscript

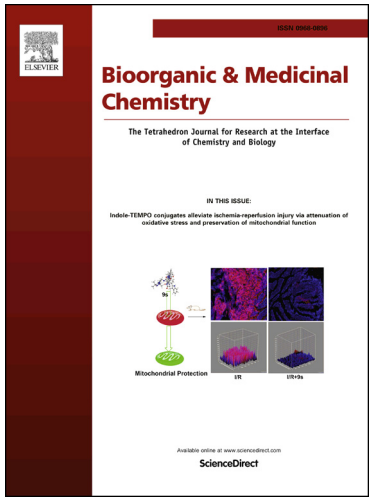

An Integrated Chemical Biology Approach Reveals the Mechanism of Action of HIV Replication Inhibitors

Nicholas Pagano, Peter Teriete, Margrith Mattman, Li Yang, Beth A. Snyder, Zhaohui Cai, Marintha L. Heil, Nicholas D.P. Cosford

PII: S0968-0896(17)30657-0
DOI: http://dx.doi.org/10.1016/j.bmc.2017.03.061
Reference: BMC 13659

To appear in: *Bioorganic & Medicinal Chemistry*

Received Date: 23 December 2016
Revised Date: 25 March 2017
Accepted Date: 29 March 2017

Please cite this article as: Pagano, N., Teriete, P., Mattman, M., Yang, L., Snyder, B.A., Cai, Z., Heil, M.L., Cosford, N.D.P., An Integrated Chemical Biology Approach Reveals the Mechanism of Action of HIV Replication Inhibitors, *Bioorganic & Medicinal Chemistry* (2017), doi: http://dx.doi.org/10.1016/j.bmc.2017.03.061

An Integrated Chemical Biology Approach Reveals the Mechanism of Action of HIV Replication Inhibitors

Nicholas Pagano[a,†], Peter Teriete[a,†], Margrith Mattman[a], Li Yang[a], Beth A. Snyder[b], Zhaohui Cai[b], Marintha L. Heil[b], and Nicholas D. P. Cosford[a,*]

[a]Cancer Metabolism & Signaling Networks Program and Conrad Prebys Center for Chemical Genomics, Sanford Burnham Prebys Medical Discovery Institute, 10901 N. Torrey Pines Rd., La Jolla, CA 92037.

[b]Southern Research Institute, Drug Development Division, 431 Aviation Way, Frederick, MD 21701.

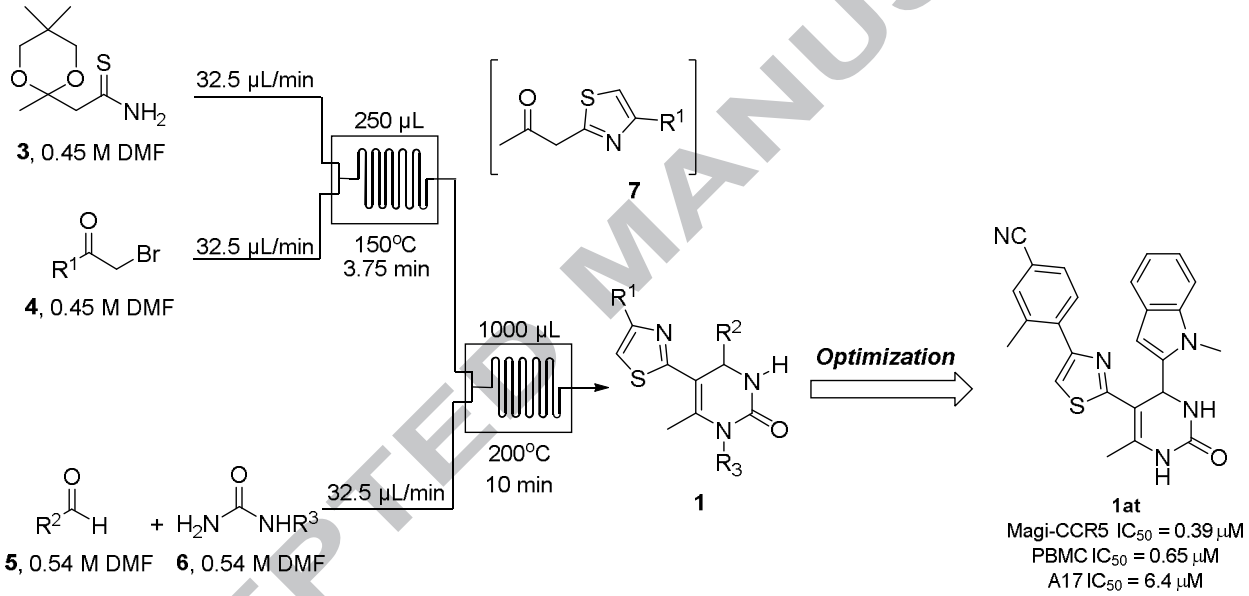

Corresponding Author: *To whom correspondence should be addressed. Tel: 858-646-3100. Fax: 858-795-5225. e-mail: ncosford@sbpdiscovery.org. †These authors contributed equally.

ABSTRACT

Continuous flow (microfluidic) chemistry was employed to prepare a small focused library of dihydropyrimidinone (DHPM) derivatives. Compounds in this class have been reported to exhibit activity against the human immunodeficiency virus (HIV), but their molecular target had not been identified. We tested the initial set of DHPMs in phenotypic assays providing a hit (**1i**) that inhibited the replication of the human immunodeficiency virus HIV in cells. Flow chemistry-driven optimization of **1i** led to the identification of HIV replication inhibitors such as **1l** with cellular potency comparable with the clinical drug nevirapine (NVP). Mechanism of action (MOA) studies using cellular and biochemical assays coupled with 3D fingerprinting and *in silico* modeling demonstrated that these drug-like probe compounds exert their effects by inhibiting the viral reverse transcriptase polymerase (RT). This led to the design and synthesis of the novel DHPM **1at** that inhibits the replication of drug resistant strains of HIV. Our work demonstrates that combining flow chemistry-driven analogue refinement with phenotypic assays, *in silico* modeling and MOA studies is a highly effective strategy for hit-to-lead optimization applicable to the discovery of future therapeutic agents.

Keywords: flow chemistry, microreactors, multistep synthesis, HIV, NNRTI, resistant virus activity, dihydropyrimidinone

1. Introduction

In broad terms the process of drug discovery can be separated into two different but well-defined approaches. The target-based approach consists of identifying a suitable protein target and screening chemical libraries of small molecules against this target to identify hits that may be optimized into drugs. The phenotypic drug discovery approach involves screening in cells or organisms where the target is unknown and the mechanism of action (MOA) of active compounds is deduced later through a process of deconvolution. More recently the use of targeted compound libraries based on so-called "privileged" scaffolds that are known to have biological activity against one target class have been used to screen against other targets to identify hits.[2-9] All of these approaches are either target-based or phenotype-based and originate in searches for small molecule therapeutic agents for a specific disease, as discussed in detail by Schenone and colleagues.[6] We have refined a different approach. Our compound-centric methodology that starts with highly promising scaffolds, identifies a putative therapeutic area where these scaffolds may prove beneficial, and subsequently identies a molecular target for the compound action. We have exemplified this novel strategy to generate new classes of bio-active compounds based on our ability to rapidly generate diverse dihydropyrimidinone (DHPM) derivatives.[10]

DHPMs are well known as privileged scaffolds that exhibit favorable therapeutic and pharmacological properties across a range of bioactivities in approved drugs.[11,12] A comprehensive analysis of published bioactivities of DHPMs with some similarity to our derivatives led us to investigate activity against human immunodeficiency virus (HIV),[13] a therapeutic target that is amenable to phenotypic screening. HIV is the causative agent of acquired immunodeficiency syndrome (AIDS), a disease for which there is no cure. Currently, more than 1.1 million people in the USA are living with HIV infection. The prevalence of

HIV/AIDS is on the rise with about 50,000 new infections each year in the USA alone. The cost of these new cases is estimated to be around $36.4 billion, comprised of both direct medical costs ($6.7 billion) and loss of productivity ($29.7 billion).[14] A comprehensive analysis of the contemporary cost of HIV healthcare by Gebo and colleagues concluded: "*HIV healthcare in the United States continues to be expensive, with the majority of expenditures attributable to medications. With improved HIV survival, costs may increase and should be monitored in the future.*"[15] Despite the fact that there are over 25 FDA approved drugs for the treatment of HIV,[16] the well-documented ability of the virus to acquire resistance against established methods of treatment requires the development of novel drug classes. There is therefore an ongoing significant need to investigate probe molecules that could ultimately lead to drugs with the capacity to overcome such resistance.[17, 18]

Herein we describe how screening a focused library of small molecule compounds in a phenotypic assay coupled with flow chemistry-driven hit-to-lead optimization, comprehensive database and computational modeling led to the prediction and subsequent identification of the MOA for a novel series of HIV replication inhibitors. Our efficient approach to target identification and validation may provide the basis for an expanded drug discovery program.

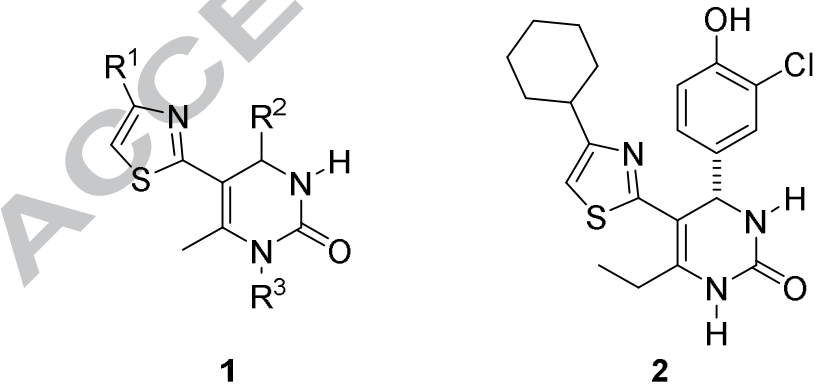

1 **2**

Figure 1. 5-(Thiazol-2-yl)-3,4-dihydropyrimidin-2(*1H*)-one derivatives.

2. Results and Discussion

We recently reported a highly efficient continuous flow method for the synthesis of substituted dihydropyrimidinone (DHPM) derivatives (**1**).[10] Our methodology provides access to a scaffold with favorable drug-like characteristics and allows the generation of highly varied analogues. The compounds prepared in this way are structurally related to thiazole derivatives such as compound **2** that were initially disclosed in a patent application and subsequently reported in the scientific literature (Figure 1).[13] We were intrigued by the physical similarity between our DHPM derivatives and the related structures **2**, which were described to possess inhibitory activity toward HIV replication in cells, although no MOA has been reported.[13] We therefore designed a biological testing funnel to narrow down the target of the DHPMs (Figure 2). We initiated target identification studies by comparing antiviral activity in two commonly used phenotypic screens. The MAGI-CCR5 antiviral assay is a single round antiviral assay employing the MAGI-CCR5 reporter cell line that produces low levels of virus. In this assay, the virus produced in an infected cell does not infect neighboring cells. MAGI-CCR5 cells can therefore be used to assess the MOA of compounds that are active early in the replication cycle, such as entry or viral reverse transcriptase polymerase (RT) inhibitors. We utilized peripheral blood mononuclear cells (PBMC) in a multi-round assay as the comparator assay.[19] In contrast to a single-round assay, in the PBMC assay the neighboring cells are infected by the progeny virions produced from the initial infection. Using control compounds as a reference, a difference of greater than two-fold activity was required in order to convince us that the activity was localized to early steps in the replication cycle. The result of this dual assay approach allowed for the confirmation of antiviral activity while already narrowing the MOA. We tested an initial set of analogues in cellular antiviral assays measuring HIV replication alongside cytotoxicity prior to

advancing to more in-depth and costly secondary studies to identify the MOA. The data generated from the first set of compounds prompted us to investigate the SAR in more detail utilizing the already established phenotypic assay and led to a new series of potent HIV replication inhibitors with drug-like properties. The most promising compound was analyzed relative to known HIV inhibitors and a hypothesis was generated that the DHPM target was the HIV RT. Molecular modeling studies along with target specific biological assays confirmed this hypothesis. Our approach to the discovery, rapid SAR and characterization of a series of new HIV replication inhibitors is described in detail below.

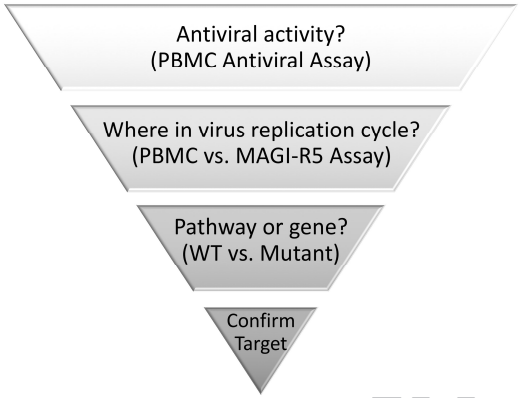

Fig 2. Testing funnel summarizing the biological assays employed in our study.

2.1. Library construction

The multistep microfluidic synthesis of DHPM analogues **1**is shown in Scheme 1[10]. At the outset of our experiments, we elected to first vary the α-bromoketones **4** to investigate the effects of changing the thiazole R^1 substituent while keeping the DHPM R^2 substituent constant (*i.e.* R^2 = 3-hydroxyphenyl). Thus, 0.75 M solutions of thioamide **3** and α-bromoketones **4** in DMF were pumped (32.5 µL/min) into a 250 µL reactor heated to 150 °C for 3.75 minutes. The stream exiting the first microreactor containing each newly constructed ketothiazole intermediate **7** was introduced to a separate stream (32.5 µL/min) of 3-hydroxybenzaldehyde **5a** and urea (**6a**) (0.90 M, DMF). The combined flow of reactants (97.5 µL/min) was pumped into a 1000 µL

reactor heated to 200 °C to generate new DHPM derivatives (**1a-1k**). Overall, the continuous two-chip microfluidic sequence required less than one hour for completion from start to finish (injection, reaction, and 1250 µL collection). The yields for the three-step (thiazole formation/deprotection/Biginelli reaction), two-chip sequence were high (39%-48%) (Table 1) and provided sufficient quantities of compounds **1a**-**1k** for characterization and evaluation in cellular antiviral assays (Table 1). Of the eleven entries, only the extremely electron poor α-bromoketone **4e** (4-trifluoromethylphenyl) failed to furnish product using this methodology and thus **1e** was prepared using a one-pot batch procedure using conditions optimized using our flow method (Scheme 4). It is notable that the reaction conditions developed for the flow method translated very successfully into batch mode.

Scheme 1. Microfluidic setup for the synthesis of DHPM analogues **1**.

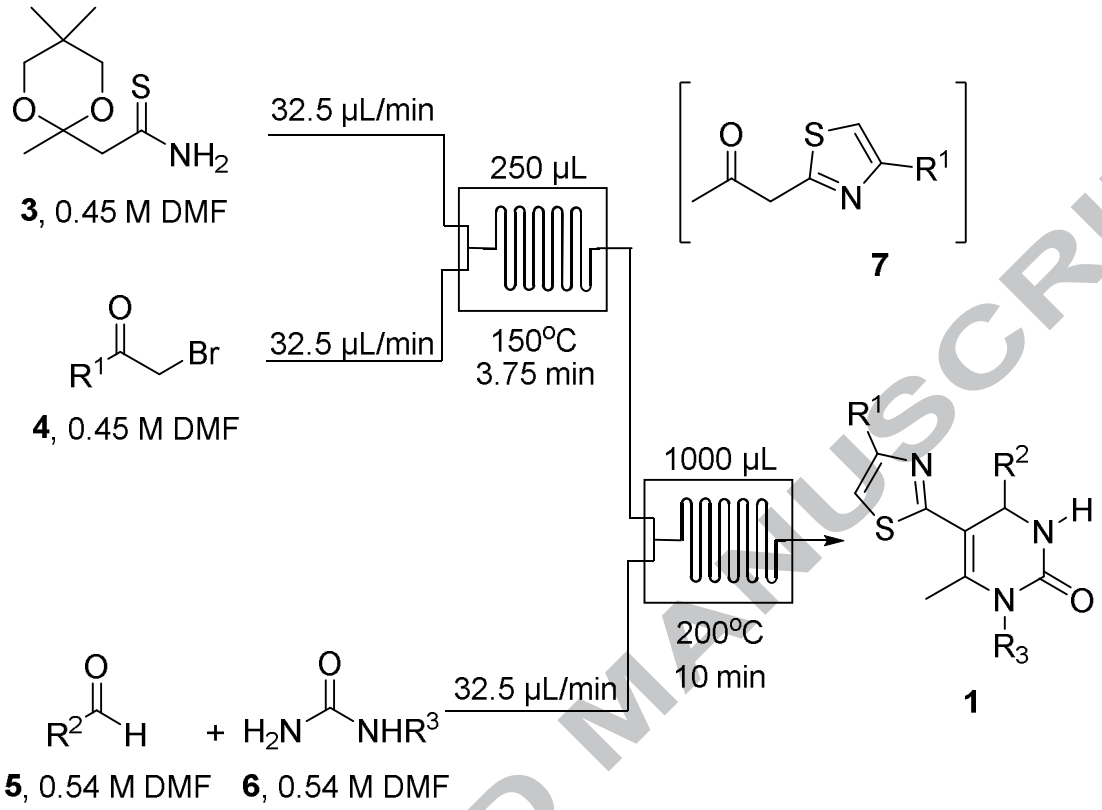

To evaluate the activity of this set of DHPMs, we assessed antiviral activity in the single round MAGI-CCR5 reporter cells and the PBMC assay. The structures of DHPMs **1a**-**1k** and their antiviral activity against HIV-$1_{Ba\text{-}L}$ replication in both MAGI-CCR5 reporter cells and also in PBMCs are presented in Table 1. Compounds that dose-dependently reduced MAGI-CCR5 β-galactoside activity with a therapeutic index (TI) ≥ 10 (*i.e.* $IC_{50} \leq 10$ µM and $TC_{50} \geq 100$ µM) were tested along with inactive and sub-optimally active compounds in the PBMC assay to confirm activity and the trend observed in the MAGI-CCR5 assay. For these experiments, the non-nucleoside RT inhibitor (NNRTI) nevirapine (NVP) was used as a reference standard. We observed that the difference in compound activity in the assays was between 2-4 fold for most

compounds in the series suggesting that the MOA of the DHPM series involved viral pathways and genes associated with virus entry or reverse transcription.

We were pleased to observe that one of our initial compounds, **1i** (4-cyanophenyl), proved to be a sub-micromolar inhibitor with an IC_{50} value of 0.44 ± 0.03 μM in the MAGI-CCR5 assay. In fact, when compared to the other compounds in this initial library, **1i** proved to be far superior with one of the lowest IC_{90} values (2.08 ± 0.32 μM) as well. In addition, and most encouraging, **1i** maintained high levels of cell viability while exhibiting a satisfactory TI of 231.3 ± 15.9. This activity of **1i** was confirmed in PBMCs demonstrating specific viral reduction and limited cell toxicity after an extended exposure in culture. Halogen substitution (entries 6-8) also yielded fairly potent compounds (**1f**-**1h**); however, this was accompanied by increased levels of cellular toxicity. Interestingly, DHPMs bearing hydrogen-bonding functional groups such as methoxy and hydroxy (**1b** and **1c**) were poor inhibitors with IC_{50} values of 66.4 ± 17.7 μM and 68.3 ± 3.9 μM, respectively in MAGI-CCR5 and 29.6 μM and 39.9 ± 6.9 μM, respectively in PBMCs. These results are especially notable because the 4-cyanophenyl moiety present in **1i** is significantly different, both sterically and electronically, from the cyclohexyl ring present at the corresponding position of compound **2** (Figure 1). Thus, we had discovered a previously unidentified structural motif that imparts potent HIV inhibitory activity.

Table 1. DHPMs **1a**-**k** and Antiviral Activity Against HIV-1 MAGI-CCR5 Cells or PBMCs.

Entry	Product	R^1	Yield (%)[a]	MAGI-CCR5[b]				PBMC[b]			
				IC_{50} (μM)	IC_{90} (μM)	TC_{50} (μM)	TI	IC_{50} (μM)	IC_{90} (μM)	TC_{50} (μM)	TI
1	1a	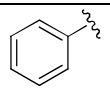	46[c]	79 ± 7.4	> 100	> 100	1.3	37 ± 8.0	81 ± 8.7	76 ± 13.1	2.0
2	1b	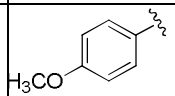	43[c]	66 ± 17.7	> 100	> 100	1.5	30[e]	78[e]	91[e]	3.0[e]
3	1c	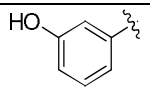	45[c]	68 ± 3.9	98 ± 0.8	89 ± 0.6	1.3	40 ± 6.9	85 ± 2.0	55 ± 7.4	1.4
4	1d	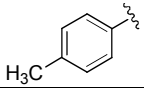	44[c]	31 ± 6.9	80 ± 2.4	61 ± 1.7	2.0	16 ± 4.0	48 ± 11.6	65 ± 2.9	4.1
5	1e	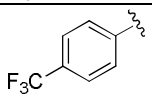	61[d]	5.2 ± 1.6	23 ± 0.5	40 ± 4.2	7.7	5.9 ± 1.3	18 ± 4.9	57 ± 1.7	9.7
6	1f	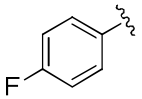	39[c]	3.8 ± 0.6	50 ± 5.4	60 ± 1.4	16	8.0 ± 4.4	18 ± 6.7	58 ± 6.8	7.3
7	1g	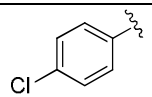	48	1.9 ± 0.3	11 ± 2.8	55 ± 2.2	29	1.3 ± 0.2	4.1 ± 0.3	65 ± 2.3	50
8	1h	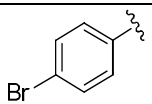	43[c]	2.3 ± 2.9	15 ± 2.9	60 ± 0.8	26	3.6 ± 11.6	12 ± 4.4	56 ± 2.5	16
9	1i	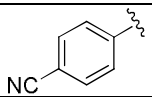	46	0.44 ± 0.03	2.1 ± 0.3	98 ± 2.1	223	0.19 ± 0.05	0.66 ± 0.07	84 ± 8.2	442
10	1j	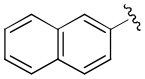	43[c]	43 ± 1.1	84 ± 0.4	55 ± 0.6	1.3	13 ± 1.5	29 ± 1.8	47 ± 6.0	3.6
11	1k	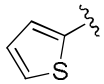	45[c]	49 ± 2.8	> 100	> 100	2.0	NT	NT	NT	NT
12	NVP	--	--	0.04 ± 0.00	0.03 ± 0.00	10	250	0.06 ± 0.01	0.18 ± 0.03	10	167

IC_{50} – compound concentration that reduces viral replication by 50%. IC_{90} – compound concentration that reduces viral replication by 90%. TC_{50} – compound concentration that reduces cell viability by 50%. Therapeutic Index (TI) = TC_{50}/IC_{50}. NT = not tested. NVP = nevirapine. [a] Isolated yields based on 1250 μL collection volumes and following silica gel chromatography. [b] An average of at least three independent experiments. [c] Flow synthesis previously reported.[10, 20] [d] Prepared using one-pot batch procedure, see Scheme 2 for details. [e] n = 1.

Having discovered an R^1 substituent (4-cyanophenyl) that imparts submicromolar potency, as in **1i**, we next focused our efforts on probing the R^2 substituent on the DHPM ring. We therefore adopted the same flow-based synthetic protocol above and shown in Scheme 1 but now with variation in the aryl aldehyde component **5**. In addition to exploring different oxo-substituted benzaldehyde precursors, we also wished to investigate whether para-cyano substitution was indeed optimal as well as the effect that *N*-methylation would have on the potency of our compounds by using methylurea (**6b**). Thus, 0.45 M solutions of thioamide **3** and α-bromoketones **4i** (4-cyanophenyl) or **4l** (3-cyanophenyl) in DMF were pumped (32.5 μL/min) into a 250 μL reactor heated to 150 °C for 3.75 minutes. Then, each newly constructed ketothiazole intermediate **7** was introduced to a separate stream (32.5 μL/min) of aldehydes **5** and either urea (**6a,** R^3 = H) or methylurea (**6b,** R^3 = Me) (0.54 M, DMF). The combined flow (97.5 μL/min) was pumped into a 1000 μL reactor heated to 200 °C. Unlike our previous setup (Scheme 1), the concentration of the reaction was lowered due to variable precipitation issues at 0.75 M. The isolated yields for the three-step, two-chip sequence were somewhat modest (22%-45%) (Table 2), the poorest results observed when using resonance-donating benzaldehydes (entries 1, 2, 4, 6, and 9). This decrease in multistep efficiency is most likely a result of less favorable imine formation in the Biginelli reaction with the electron-rich aldehydes.

The structures of DHPMs **1l**-**1w** and their antiviral activity against HIV-$1_{Ba\text{-}L}$ in MAGI-CCR5 reporter cells and PBMCs are presented in Table 2. Overall, most benzaldehyde components leading to para-oxygen substituted R^2 moieties yielded compounds with improved levels of potency with IC_{50} values < 0.15 μM (**1l**, **1m**, **1p** and **1q**). We were pleased to observe that only one of these compounds (**1m**) decreased cell viability to any significant extent as measured by the MAGI-CCR5 TC_{50} value. 4-Cyanophenyl substitution proved superior to 3-cyanophenyl substitution, which led to decreased potency and increased toxicity levels (**1t** and **1u**), while methyl substitution at R^3 (**6b**) also provided much poorer inhibitory activity in cells (**1v** and **1w**). Lastly, these data helped us to develop two hypotheses. The first was that relatively bulky R^2 substituents were well tolerated. Both **1p** (phenoxy) and **1q** (benzyloxy) proved to be among our best compounds up to this point. The second was that, at a minimum, a hydrogen-bond acceptor is important for attaining increased levels of potency. The molecular modeling studies described below support both of these ideas.

Table 2. DHPMs **1l-1w** and Antiviral Activity Against HIV-1 MAGI-CCR5 Cells or PBMCs.

Entry	Product	Yield (%)[a]	R^2	R^1	R^3	MAGI-CCR5[b]				PBMC[b]			
						IC_{50} (μM)	IC_{90} (μM)	TC_{50} (μM)	TI	IC_{50} (μM)	IC_{90} (μM)	TC_{50} (μM)	TI
1	**1l**	22	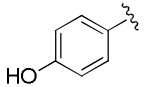	4-CNPh	H	0.04 ± 0.00	0.52 ± 0.15	> 10.00	250	0.04 ± 0.00	0.12 ± 0.02	> 100.00	2500
2	**1m**	27	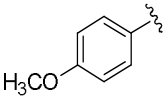	4-CNPh	H	0.08 ± 0.01	0.37 ± 0.07	7.0 ± 1.3	88	0.12 ± 0.02	0.30 ± 0.03	76.6 ± 23.4	638
3	**1n**	35	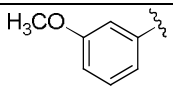	4-CNPh	H	0.38 ± 0.04	1.8 ± 0.4	> 100.00	263	0.56 ± 0.16	1.6 ± 0.5	> 100.00	179
4	**1o**	22	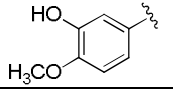	4-CNPh	H	0.38 ± 0.06	37.8 ± 31.1	> 100.00	263	0.15 ± 0.01	0.42 ± 0.06	> 100.00	667
5	**1p**	33	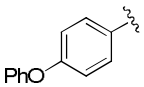	4-CNPh	H	0.12 ± 0.02	0.62 ± 0.04	> 10.00	83	0.53 ± 0.08	1.8 ± 0.4	> 100.00	189
6	**1q**	30	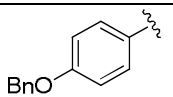	4-CNPh	H	0.13 ± 0.01	0.75 ± 0.01	> 10.00	77	0.21 ± 0.10	0.60 ± 0.30	> 100.00	476
7	**1r**	40	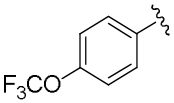	4-CNPh	H	1.6 ± 0.3	7.6 ± 0.9	> 100.00	63	8.6 ± 3.3	21.0 ± 6.8	> 100.00	12
8	**1s**	45	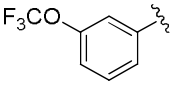	4-CNPh	H	2.4 ± 0.6	69.8 ± 30.2	> 100.00	42	41.2 ± 21.9	> 100.00	> 100.00	2.4
9	**1t**	27	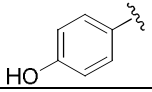	3-CNPh	H	4.4 ± 0.6	40.9 ± 1.5	69.6 ± 4.8	16	3.3 ± 1.2	10.2 ± 1.7	87.5 ± 12.5	27
10	**1u**	26	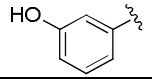	3-CNPh	H	8.7 ± 1.0	38.1 ± 2.7	51.8 ± 5.9	6.0	5.0 ± 1.4	15.1 ± 4.1	74.0 ± 16.2	15
11	**1v**	35	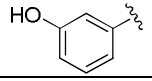	3-CNPh	Me	55.4 ± 2.4	89.2 ± 0.5	> 100.00	1.8	14.5 ± 1.5	59.6 ± 4.6	64.2 ± 10.3	4.4
12	**1w**	28	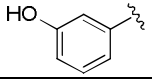	4-CNPh	Me	2.4 ± 0.9	13.8 ± 6.2	> 100.00	42	3.2 ± 0.1	8.5 ± 0.1	> 100.00	31
13	**NVP**	--	--	--	--	0.04 ± 0.00	0.42 ± 0.03	10.0 ± 0.0	250	0.06 ± 0.01	0.19 ± 0.03	10.0 ± 0.0	167

IC_{50} – compound concentration that reduces viral replication by 50%. IC_{90} – compound concentration that reduces viral replication by 90%. TC_{50} – compound concentration that reduces cell viability by 50%. TI = TC_{50}/IC_{50}. NT = not tested. NVP = nevirapine. [a] Isolated yields based on 1250 μL collection volumes and following silica gel chromatography. [b] An average of at least three independent experiments.

We next investigated the incorporation of heteroatoms into the aryl substituent R^2 by selecting the appropriate aldehyde building blocks **5**. While we were encouraged by both the potency and toxicity profiles of our best compounds up to this point, the majority of them remained relatively hydrophobic and we therefore aimed to improve the drug-like properties of the scaffold. For the microfluidic synthesis of this set of analogues α-bromoketone **4i** (R^1 = 4-cyanophenyl) was used in combination with various heteroaryl aldehydes **5**. While the overall yield for this continuous sequence was high (34%-46%) (Table 3), only pyridine substitution proved viable under these conditions. Even at decreased reaction concentrations (0.45 M), extended heterocyclic substrates failed to yield products (**1aa**-**1ad**) often precipitating within the second microreactor chip. Thus, similar to **1e**, these four compounds were prepared using a one-pot, batch-mode procedure (Scheme 2). Overall, these unfunctionalized heterocycles possessed relatively good potency, with *N*-methylindole **1ad** reaching the nanomolar range with an IC_{50} value of 0.74 μM ± 0.17. Furthermore, only one entry displayed any level of cellular toxicity (**1ac**).

Table 3. DHPMs **1x-1ad** and Antiviral Activity Against HIV-1 MAGI-CCR5 Cells or PBMCs.

Entry	Product	Yield (%)	R^2	MAGI-CCR5[c]				PBMC[c]			
				IC_{50} (μM)	IC_{90} (μM)	TC_{50} (μM)	TI	IC_{50} (μM)	IC_{90} (μM)	TC_{50} (μM)	TI
1	1x	34[a]	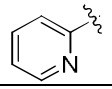	2.0 ± 0.5	> 100.00	> 100.00	50	1.3 ± 0.5	4.4 ± 2.1	> 100.00	77
2	1y	39[a]	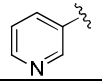	2.9 ± 0.1	> 100.00	> 100.00	35	1.5 ± 0.4	14.3 ± 5.5	> 100.00	67
3	1z	46[a]	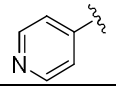	1.4 ± 0.4	> 100.00	> 100.00	71	0.80 ± 0.20	34.6 ± 32.7	> 100.00	125
4	1aa	51[b]	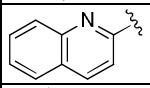	3.8 ± 1.0	98.3 ± 1.7	> 100.00	26	2.9 ± 0.9	10.5 ± 4.0	68.3 ± 22.1	24
5	1ab	56[b]	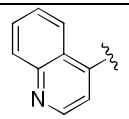	1.5 ± 0.3	12.7 ± 3.6	> 100.00	67	1.3 ± 0.2	5.5 ± 0.8	> 100.00	77
6	1ac	38[b]	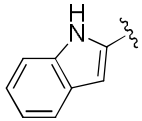	2.1 ± 0.4	10.4 ± 1.4	50.5 ± 7.3	24	3.5 ± 1.8	10.8 ± 4.8	69.8 ± 16.5	20
7	1ad	20[b]	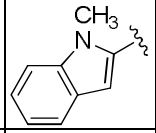	0.7 ± 0.1	3.7 ± 0.7	> 100.00	143	1.1 ± 0.3	3.2 ± 0.5	> 100.00	91
8	NVP	--	--	0.04 ± 0.00	0.42 ± 0.03	10.0 ± 0.0	250	0.06 ± 0.01	0.19 ± 0.03	10.0 ± 0.0	167

IC_{90} – compound concentration that reduces viral replication by 90%. TC_{50} – compound concentration that reduces cell viability by 50%. TI = TC_{50}/IC_{50}. NVP = nevirapine. [a] Isolated yields based on 1250 μL collection volumes and following silica gel chromatography. [b]Prepared using one-pot procedure, see Scheme 2 for details. [c] An average of at least three independent experiments. IC_{50} – compound concentration that reduces viral replication by 50%.

Although the latest round of cellular data (Table 3) suggested that indole derivatives (**1ac** and **1ad**) showed promising HIV inhibitory activity we elected to further investigate additional SAR around the pyridine series. Fortunately, a considerable number of substituted pyridyl aldehydes are commercially available allowing us to access these structures rapidly. Thus we constructed DHPMs **1ae**-**1as** all from α-bromoketone **4i** (R1 = 4-cyanophenyl) and the results along with their antiviral activity against HIV-1 MAGI-CCR5 cells are presented in Table 4. The overall yield for this three-step, two-chip microfluidic sequence was high (42%-64%) with only six examples (entries 6, 10-13, 15) requiring a one-pot batch preparation due to precipitation inside the microchip. Initially, perhaps most impressive is that all 15 pyridyl entries do not display any measureable levels of cellular toxicity. The combination of the nitrogen heteroatom with either *para* alkoxy- (**1an**) or aryloxy- (**1as**) yielded several sub-micromolar inhibitors.

Table 4. DHPMs **1ae**-**1at** and Antiviral Activity Against HIV-1 MAGI-CCR5 Cells or PBMCs.

Entry	Product	Yield (%)[a]	R^2	MAGI-CCR5[c]				PBMC[c]			
				IC_{50} (μM)	IC_{90} (μM)	TC_{50} (μM)	TI	IC_{50} (μM)	IC_{90} (μM)	TC_{50} (μM)	TI
1	1ae	45[a]	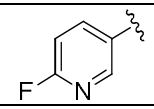	1.1 ± 0.1	5.4 ± 0.7	> 100	91	0.59 ± 0.13	2.0 ± 0.3	> 100	170
2	1af	64[a]	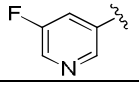	0.7 ± 0.1	> 100.00	> 100	143	0.53 ± 0.17	1.3 ± 0.6	> 100	189
3	1ag	49[a]	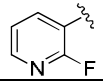	0.44 ± 0.07	2.6 ± 0.4	> 100	227	0.26 ± 0.04	0.83 ± 0.03	> 100	385
4	1ah	59[a]	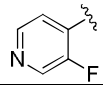	63.4 ± 20.0	> 100.00	> 100	1.6	NT	NT	NT	
5	1ai	47[a]	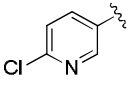	0.48± 0.08	2.4 ± 0.6	> 100	208	0.38 ± 0.06	0.94 ± 0.03	> 100	263
6	1aj	54[b]	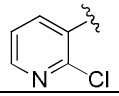	2.2 ± 0.5	85.5 ± 14.5	> 100	46	1.5 ± 0.7	8.8 ± 6.2	> 100	67
7	1ak	38[a]	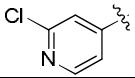	3.2 ± 1.0	> 100.00	> 100	31	4.4 ± 1.4	44.5 ± 28.2	> 100	23
8	1al	42[a]	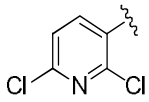	0.86 ± 0.02	5.8 ± 0.4	> 100	116	1.9 ± 0.7	5.7 ± 1.5	99.1 ± 0.9	52
9	1am	47[a]	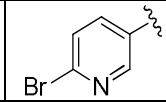	0.35 ± 0.02	1.4 ± 0.3	> 100	286	0.21 ± 0.09	0.57 ± 0.19	> 100	476
10	1an	48[b]	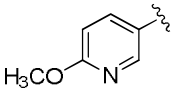	0.10 ± 0.02	0.58 ± 0.13	> 10.0	100	0.12 ± 0.01	0.43 ± 0.09	> 100	833
11	1ao	48[b]	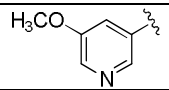	10.4 ± 3.0	> 100.00	> 100	9.6	NT	NT	NT	
12	1ap	57[b]	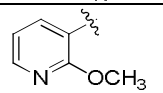	3.8 ± 0.8	66.0 ± 20.4	> 100	26	2.6 ± 0.6	7.3 ± 1.2	> 100	39
13	1aq	37[b]	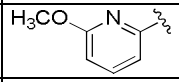	1.6 ± 0.3	14.4 ± 3.0	> 100	63	1.6 ± 0.7	5.9 ± 1.5	> 100	63
14	1ar	54[a]	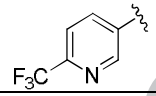	1.1 ± 0.3	7.3 ± 0.8	> 100	91	1.2 ± 0.8	4.6 ± 1.9	> 100	83

15	**1as**	33[b]	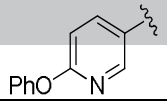	0.64 ± 0.04	2.8 ± 0.1	> 100	156	1.2 ± 0.3	3.4 ± 0.8	67.5 ± 17.8	56
16	**1at**	30[b]	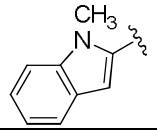	0.39 ± 0.05	1.9 ± 0.3	> 100	256	0.65[d]	2.17[d]	> 100[d]	154
NVP	**--**	--	--	0.04 ± 0.00	0.42 ± 0.03	10.0 ± 0.0	250	0.06 ± 0.01	0.19 ± 0.03	10 ± 0.0	167

IC_{50} – compound concentration that reduces viral replication by 50%. IC_{90} – compound concentration that reduces viral replication by 90%. TC_{50} – compound concentration that reduces cell viability by 50%. TI = TC_{50}/IC_{50}. NT = not tested. NVP = nevirapine. [a] Isolated yields based on 1250 µL collection volumes and following silica gel chromatography. [b]Prepared using one-pot batch procedure, see Scheme 2 for details. [c]An average of at least three independent experiments. [d]n = 1.

As mentioned previously, a "one-pot" batch-mode procedure was necessary for the production of certain target DHPMs **1**. Even at reduced concentrations (0.45 M), several reaction sequences suffered from irregular precipitation inside the second microchip. Thus, we developed an in-flask batch procedure to access these compounds and this one-pot process is shown in Scheme 2. Unlike our automated flow procedure, the batch process does not facilitate rapid high-throughput synthesis. However, the batch method does allow us to conduct transformations using heterogeneous conditions at much higher concentrations to target specific analogues as needed. In summary, utilizing alternative methodologies allowed us to quickly access most substitution patterns of interest.

Scheme 2. "One-pot" batch synthesis of DHPMs **1**.

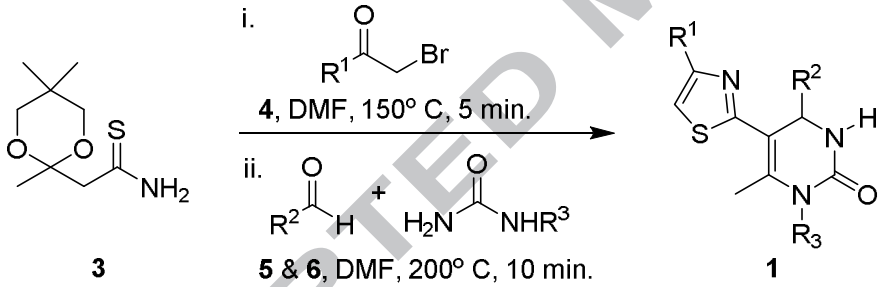

At this stage we had synthesized more than forty DHPMs and tested them extensively in cellular assays measuring the inhibition of HIV replication and found several analogues with submicromolar potency. We next tested some of the most promising compounds to assess their drug-like properties *in vitro* using absorption, distribution, metabolism, and excretion (ADME) assays. The results of these studies are shown in Table 5. Permeability was assessed via a parallel artificial membrane permeability assay that estimates blood brain barrier penetration (BBB-PAMPA). The results suggested that the DHPMs are likely to exhibit poor CNS permeability *in*

vivo.[21] The data for plasma and microsomal stability were very encouraging, with all compounds exhibiting good to excellent parameters. Taken together, the *in vitro* ADME data suggest that compounds in this series are likely to have drug-like properties suitable for *in vivo* proof-of-concept studies.

Table 5. *In vitro* ADME data for selected DHPMs.

Entry	Cpd	R^2	PAMPA (LogPe)[a]	Plasma Stability[b] (%)	Microsomal Stability[b] (%)
1	1i	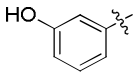	-7.84 ± 0.22	88.46 ± 10.73	52.35 ± 0.71
2	1l	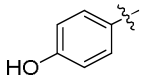	-7.82 ± 0.14	100.00 ± 8.50	100.00 ± 4.60
3	1m	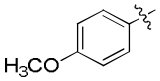	-7.11 ± 0.06	95.97 ± 1.36	63.15 ± 4.43
4	1y		-7.50 ± 0.10	89.42 ± 2.93	75.55 ± 7.86
5	1ad	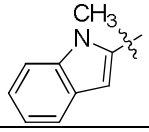	-7.05 ± 0.12	95.63 ± 4.19	62.87 ± 1.40
6	1ai	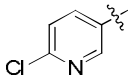	-7.40 ± 0.03	91.65 ± 2.56	63.40 ± 0.73
7	1ae	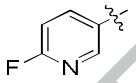	-6.24 ± 0.07	100.00 ± 6.37	49.38 ± 1.00
8	1an	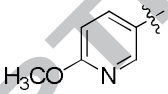	-7.25 ± 0.05	100.00 ± 18.70	69.42 ± 1.94
9	1am	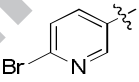	-7.82 ± 0.05	98.29 ± 8.08	67.61 ± 1.35

[a]Permeability is monitored by measuring the amount of compound that can diffuse through a polar brain lipid membrane to predict BBB permeability. [b]Percent remaining after incubation for 60 min. at 37 °C.

2.2. Mechanism of Action, Biological Relevance and the *In Silico*-Guided Design of a New Inhibitor (1at).

Given the potency, ability to rapidly produce derivatives and identification of unique structural motifs, we concluded that molecular modeling and secondary biological studies to identify the direct protein target of the DHPMs were warranted. Comparison of our compounds with the NNRTIs rilpivirine and etravirine, using *in silico* modeling, suggested some apparent similarities in the structures and possible overlap of pharmacophoric features (Figure 3; Table 6). We therefore sought experimental confirmation by first probing activity against viruses with mutations in the NNRTI binding pocket followed by assessment of DHPMs binding to the viral RT.

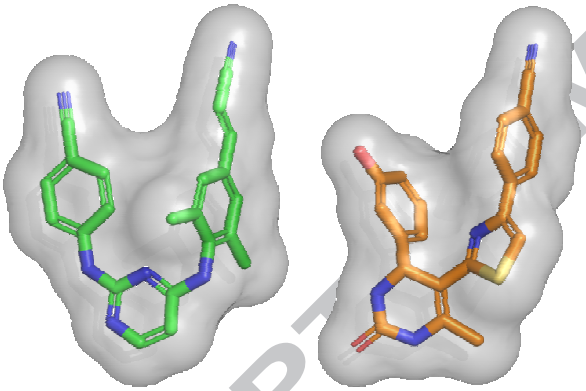

Figure 3. Small molecule steric alignment based on the active conformation of rilpivirine (green) and compound **1i** (orange) (Discovery Studio 3.0; Accelrys, San Diego, CA).

Compound	Rilpivirine	Etravirine
(*R*)-1i	0.807	0.776
(*S*)-1i	0.805	0.796
(*R*)-1an	0.820	0.780
(*S*)-1an	0.813	0.798

Table 6. Molecular steric alignment similarity between the stereoisomers of two DHPM analogues and the NNRTIs rilpivirine and etravirine in their active conformation[1] (Discovery Studio 3.0; Accelrys, San Diego, CA).

The advent of highly active anti-retroviral therapy (HAART) for the chronic suppression of HIV replication in AIDS patients has dramatically increased the mean survival time and improved the quality of life for individuals infected with HIV. Prophylactic administration of

anti-retroviral therapy has been shown to reduce the risk of acquiring an infection in healthy individuals.[22-29] Furthermore, administration of the anti-retroviral drug nevirapine to pregnant women intrapartum and neonatally has been shown to successfully prevent transmission to infants.[30] In an effort to eliminate new infections in children, this treatment was expanded and it is now recommended that HIV infected pregnant women are provided lifelong anti-retroviral therapy as well as postpartum administration of a single dose of nevirapine or AZT from birth through age 4-6 weeks for the child.[31-34] In 2012, the prophylactic administration of anti-retroviral therapy was approved for the prevention of infection of healthy individuals at high risk of contracting the disease.[35] Now more than ever, millions of infected and uninfected people are relying on lifelong anti-retroviral agents until a sterilizing cure can be identified.

The HIV RT is an RNA-dependent DNA polymerase that transcribes the viral RNA into double-stranded proviral DNA copy. The RT has three functions: (1) transcription of the viral RNA into DNA; (2) cleavage of the viral RNA by Ribonuclease H; and (3) transcription of the second DNA strand. The RT is a heterodimer composed of two subunits p66 and p51. The 440 N-terminal amino acids of the p66 subunit functions as the viral polymerase and the C-terminal 120 amino acids function as the ribonuclease. The p51 subunit contains the same 440 N-terminal amino acids found in the p66 subunit. NNRTIs are allosteric inhibitors of RT polymerization. Structural studies of RT in complex with NNRTIs reveal that inhibitors bind into a pocket primarily composed of amino acids residues Lys101, Lys103, Tyr181, Tyr188, Phe227, Trp229, and Tyr318.[1, 36-40] NNRTI binding is non-catalytic and non-competitive; therefore, the combination of the small molecule surface contact and flexibility influence the potency of the inhibitors.[41-44]

Several DHPMs with potent activity in cells and low toxicity were selected for more extensive biological and *in silico* modeling studies. For the biological studies, we tested **1l**, **1m**, **1ad, 1ae, 1am, 1an** and **1ar** against A17, a virus that has amino acid variations at positions 103 and 181 (K103N and Y181C) in the NNRTI binding pocket relative to wild type. The asparagine variation at residue 103 and the cysteine variation at residue 181 are known to alter the non-nucleoside inhibitor binding-pocket sufficiently to disrupt the binding of NNRTIs such as nevirapine. Therefore, loss of antiviral activity against the virus would suggest the DHPM was binding the RT. As shown in Table 7, the K103N and Y181C mutations in the A17 virus greatly affect if not abolish the antiviral activity of the DHPMs tested in cells.

Table 7. DHPMs and inhibitory activity against HIV wildtype (NL4-3) and A17 (K103N, Y181C) virus in MAGI-CCR5 cells.

Compound	Virus	IC_{50} (μM)	IC_{90} (μM)	TC_{50} (μM)	TI
1l	NL4-3	0.06 ± 0.01	0.62 ± 0.09	46 ± 6.1	765
	A17	28 ± 1.4	95 ± 2.6		1.6
1m	NL4-3	0.05 ± 0.01	0.62 ± 0.04	5.5 ± 1.0	110
	A17	3.4 ± 0.1	24 ± 8.0		1.6
1ad	NL4-3	0.52 ± 0.15	5.0 ± 2.3	> 100	192
	A17	> 100	> 100		1
1ae	NL4-3	1.1 ± 0.2	7.6 ± 0.2	> 100	> 91
	A17	> 100	> 100		NA
1am	NL4-3	0.50 ± 0.14	3.2 ± 1.0	> 100	> 200
	A17	> 100	> 100		1
1an	NL4-3	< 0.32 ± 0.0	1.9 ± 0.9	> 100	> 313
	A17	> 100	> 100		1
1ar	NL4-3	0.86 ± 0.24	7.7 ± 1.1	> 100	> 116
	A17	> 100	> 100		NA
NVP	NL4-3	0.04 ± 0.0	0.54 ± 0.01	> 10	> 250
	A17	> 10	> 10		1

IC_{50} - compound concentration that reduces viral replication by 50%. IC_{90} - compound concentration that reduces viral replication by 90%. TC_{50} - compound concentration that reduces cell viability by 50%. TI = TC_{50}/IC_{50}. NVP = nevirapine.

For *in silico* modeling studies, compounds **1i**, **1l**, **1m**, **1y**, **1ad, 1ae, 1ai,** and **1an** were docked into the NNRTI binding pocket of wild-type (PDB code 3MEC, 3MEE, 2ZD1) as well as Y181C, K103N (PDB code 4I2Q and 4I2P) mutant forms of the RT to identify other potential interactions between RT and the DHPMs as well as gain insight into the possible orientation of the scaffold (data not shown).[45] The results of these studies indicated that the docked poses of the DHPMs aligned well with the orientation of etravirine and rilpivirine in the NNRTI binding pocket, matching the steric alignment performed previously (Figure 3; Table 7).

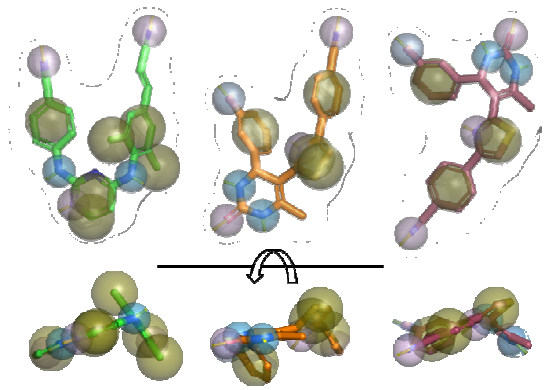

Figure 4. Small molecule alignment focusing on pharmacophore features between rilpivirine (green) and the two stereo-isomers of compound **1i** (*R* = orange and *S* = purple; Discovery Studio 3.0; Accelrys, San Diego, CA). The VDW surface is shown in transparent gray. Yellow-green sphere: hydrophobic centroids, including aromatic rings. Blue spheres: hydrogen-bond donors. Purple spheres: hydrogen-bond acceptors. Blue-Purple spheres: hydrogen-bond acceptors and donors.

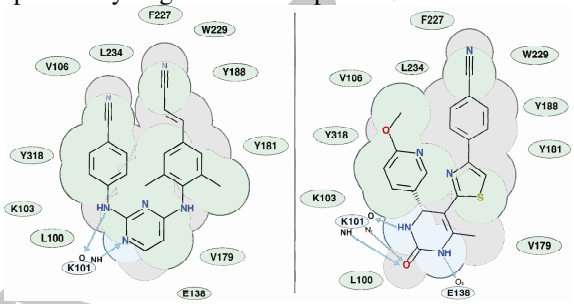

Figure 5. Molecular interaction between ripilvirine or (*R*)-**1i** and the NNRTI-site. Green shading represents hydrophobic region. Blue shading represents hydrogen bond acceptor. Cyan arrows represent hydrogen bonds (donor to acceptor). Grey parabolas represents accessible surface for large areas. Broken thick line around ligand shape indicates accessible surface. Size of residue ellipse represents the strength of the contact (Table ST3). 2D distance between residue label and ligand represents proximity (ICM, Molsoft, San Diego)

A single chiral center in the DHPM structure gives rise to two enantiomers in the racemate. In order to predict differences in activity of each enantiomer we performed another alignment *in silico*, this time taking additional pharmacophoric features into account. The differences between (*R*)-**1i** and (*S*)-**1i** when aligned with rilpivirine are shown in Figure 4. It is noteworthy here that the steric as well as pharmacophoric alignments for the (*R*)-**1i** result

Compound	ReRank Score
(*R*)-1i	**-132.1**
(S)-1i	-94.5
(*R*)-1an	**-136.4**
(*S*)-1an	-83.1

Table 8. Docking results from the stereoisomers of compounds **1i** and **1an** in the NNRTI binding site of HIV-RT from the rilpivirine structure[1] (PDB code 3MEE (Molegro MVD, Aarhus, Denmark).

in a near identical conformation. Subsequently, both enantiomers were docked into the NNRTI binding-site of wild type (WT) reverse transcriptase taken from the rilpivirine PDB submission (code 3MEE) (Molegro MVD, Aarhus, Denmark). The resulting poses were ranked based on the docking score and conformational similarity to the alignment in Figure 4 (Table 8). The results suggest a clear separation of activity between the two enantiomers, with (*R*)-**1i** being strongly favored. In support of these data the relevant amino acid interactions of ripilvirine compared with (*R*)-**1i** within the non-nucleoside binding site of the HIV RT are shown in Figure 5.

In order to support our mechanistic hypothesis, the activities of selected DHPM derivatives were confirmed in a biochemical RT assay using a method described previously[46] (Table 9). Using a chiral column, the enantiomers of compound **1i** were separated and individually tested in the MAGI-CCR5 cellular assay. Each enantiomer, (***R***)**-1i** and *(**S**)*-**1i**, was also evaluated in the PBMC cellular assay and an HIV RT biochemical assay. Compound (***R***)**-1i** was found to inhibit virus replication and polymerization of the HIV RT in a dose-dependent manner whereas *(**S**)*-**1i** had no activity (Table 9). These results further support our hypothesis that the MOA of the DHPMs is through inhibition of the viral RT at the NNRTI site. The data also support the proposed active conformations for the DHPMs determined by *in silico* modeling. All together, these studies demonstrate that, like nevirapine, the MOA of the DHPMs is through inhibition of the HIV RT and strongly suggest that the NNRTI binding pocket is the site of compound binding.

Table 9. DHPM enantiomers (*R*)-**1i** and *(S)*-**1i** and their respective inhibitory activity against HIV-1 reverse transcriptase (RT).

Product	PBMC Antiviral Assay				RT Biochemical
	IC_{50} (μM)	IC_{90} (μM)	TC_{50} (μM)	TI	IC_{50} (μM) ± SD
Nevirapine	0.04 ± 0.003	0.17 ± 0.12	> 10	> 250	0.18 ± 0.01
(*R*)-**1i**	0.11 ± 0.05	0.42 ± 0.24	> 100	> 909	0.60 ± 0.09
(S)-**1i**	22 ± 1.5	77 ± 3.4	> 100	> 4.5	Not active

Further investigation of DHPM poses docked on the crystal structure of WT RT bound to etravirine and rilpivirine respectively (PDB code 3MEC, 3MEE;[1] and PDB code 2ZD1[47]) highlighted several key interactions observed in almost all calculated poses for **1i**, **1l**, **1m**, **1y**, **1ad**, **1ae**, **1ai**, **1am**, and **1an**. First, the carbonyl group of the pyrimidinone ring interacts with the backbone amide of K103 or N103, respectively. Second, the nitrogen in the 5 position of the pyrimidinone forms an interaction with the backbone carbonyl of residue 103, while the nitrogen in the 1-position forms an interaction with the side chain carbonyl of E138 from the p51 subunit. Third, the thiazole ring shows a consistent interaction with the β-methylenes of Y181 and the non-polar side chain of V179. Fourth, the cyanophenyl ring interacts with the NNRTI binding pocket at amino acids Y181, Y188, F227, W229 and V106 (Figure S1; see Supplementary Data). This part of the NNRTI binding pocket can accommodate reasonably bulky groups, such as the cyclohexyl group in compound **2**. However, the planar shape of the phenyl ring in our series of DHPMs adds an additional π-stacking interaction with the aromatic sidechain of Y188, while the polar property of the cyano group in the 4-position can contribute through its interaction with the solvent space in the DNA binding groove. Comparing this to etravirine and rilpivirine bound to the same structures it is evident that the bulk of the DHPM binding is driven by ligand to backbone interactions. Upon closer investigation, we concluded that the NNRTI binding pocket

could be further filled by introduction of a methyl group on the 4–cyanophenyl moiety of the DHPM. We postulated that this methyl group would interact with the β-methylenes of tyrosine 183 and tryptophan 229 enabling the compound to bind to the RT with some possible variations at the residues in these positions. Based on the in silico modeling studies 3-methyl-4-(2-(6-methyl-4-(1-methyl-1H-indol-2-yl)-2-oxo-1,2,3,4-tetrahydropyrimidin-5-yl)thiazol-4-yl)benzonitrile (**1at**) was synthesized. Thus, as shown in Scheme 3, the preparation of 4-acetyl-3-methylphenyl trifluoromethanesulfonate from 1-(4-hydroxy-2-methylphenyl)ethan-1-one proceeded under standard conditions. Introduction of the nitrile was achieved through palladium catalyzed coupling of zinc cyanide with the triflate to afford 4-acetyl-3-methylbenzonitrile. Bromination of this material then provided 4-(2-bromoacetyl)-3-methylbenzonitrile which was employed in the batch synthesis of **1at** as shown in Scheme 4. The data for the initial biological evaluation of **1at** are included in Table 4, indicating that the compound exhibits sub-micromolar potency in both of the primary cellular assays.

Scheme 3. Batch synthesis of 4-(2-bromoacetyl)-3-methylbenzonitrile.

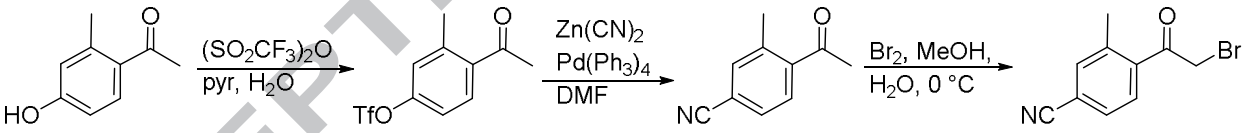

Scheme 4. Batch synthesis of 3-methyl-4-(2-(6-methyl-4-(1-methyl-1H-indol-2-yl)-2-oxo-1,2,3,4-tetrahydropyrimidin-5-yl)thiazol-4-yl)benzonitrile (**1at**).

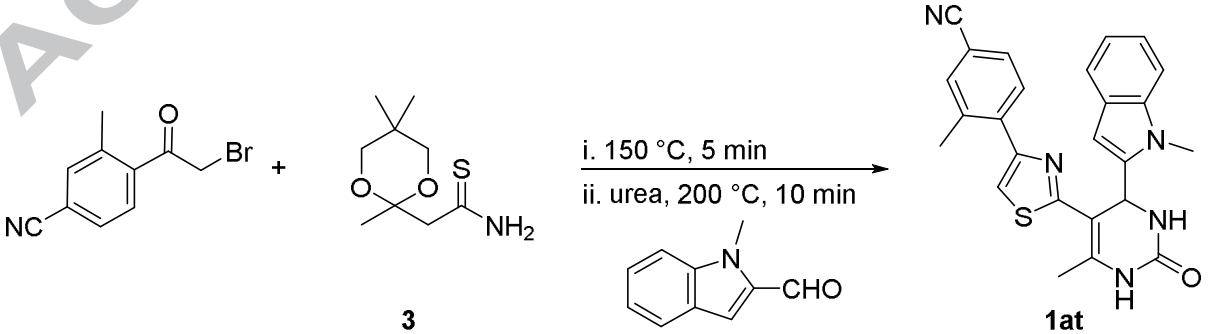

Activity against NNRTI resistant virus is an important feature of a compound with promise for further development. Mutations at the two amino acid positions, Y181C and K103N, have been associated with resistance to most NNRTIs.[48] The docking of the DHPM **1at** containing the 4-cyanophenyl moiety into the crystal structures of Y181C, K103N RT bound to rilpivirine and two analogues (Figure S2; see Supplementary Data) (PDB code 3BGR[47] and PDB codes 4I2Q, 4I2P[49]) show that favorable interactions between Y181C, K103N and the DHPM would still be feasible. Consistent with our hypothesis, we found that addition of a methyl group on the cyanophenyl ring (as in **1at**) resulted in activity against NNRTI resistant virus (A17) while maintaining potency against wild type virus (see Table 10). Importantly, compound **1at** exhibits micromolar activity against the A17 strain whereas nevirapine is essentially inactive. Based on these results we expanded testing to include cell lines with another, highly clinically relevant, mutant form of RT (E138A) and were able to detect activity against this form of RT as well (Table ST1; see Supplementary Data). It is noteworthy that our approach allowed the rapid design of analogues with an activity profile matching that of nevirapine, a standard of care drug still commonly used in triple combination therapy.[50]. Taken together, the results of these experiments suggest that the DHPMs are small molecule HIV replication inhibitors with the potential to treat resistant strains of virus.

Table 10. DHPMs **1ad & 1at** and inhibitory activity against HIV wildtype (NL4-3) and A17 (K103N, Y181C) in MAGI-CCR5.

Compound	Virus	IC_{50} (μM)	IC_{90} (μM)	TC_{50} (μM)	TI
1ad	NL4-3	0.52 ± 0.16	5.0 ± 2.3	> 100	> 192
	A17	> 100	> 100	> 100	1
1at	NL4-3	0.39 ± 0.05	4.8 ± 0.6	> 100	> 256
	A17	6.4 ± 0.6	>100	> 100	> 15.6
NVP	NL4-3	0.07 ± 0.03	0.60 ± 0.07	> 10	> 143
	A17	> 10	> 10	> 10	1

IC_{50} - compound concentration that reduces viral replication by 50%. IC_{90} - compound concentration that reduces viral replication by 90%. TC_{50} - compound concentration that reduces cell viability by 50%. TI = TC_{50}/IC_{50}. NVP = nevirapine.

3. Conclusion

Using the workflow shown in Figure 6 we rapidly identified a DHPM derivative with activity against a deadly disease (AIDS) that has desirable drug-like properties as well as chemical features ideal for synthesis but for which the molecular target was unknown. Elucidation of the MOA was essential for advancement of this molecule. Flow chemistry methods were employed for rapid hit-to-lead optimization to provide novel HIV replication inhibitors, such as **1l**, with cellular activity comparable with the clinically used drug NVP, and no detectable cytotoxicity. Using predictive *in silico* modeling combined with data from cellular and biochemical assays the compounds were shown to inhibit the viral RT enzyme. Our *in silico* model suggested that modifications to the DHPMs would provide inhibitors of drug resistant RT while maintaining activity against wild type RT. This led to the design, synthesis and testing of **1at**, a compound that, unlike NVP, inhibits the replication of the mutant HIV strains K103N and Y181C that contain amino acid variations associated with drugs exhibiting resistance to NNRTIs. Furthermore, evaluation of several active analogues in *in vitro* ADME assays suggest that these

probe compounds may have promising drug-like properties. This is especially relevant because the penetration of drugs into CNS, gut and lymphoid tissue is an important feature of future HIV therapeutics.[51-55] In summary, our work has demonstrated an efficient approach to small molecule probe discovery that combines optimization using flow synthesis[10, 20, 56] with biological testing and *in silico* modeling to achieve rapid and efficient MOA determination. Thus, we have implemented a powerful strategy that should translate to other important therapeutics targets.

Figure 6: Schematic of the compound-centric approach.

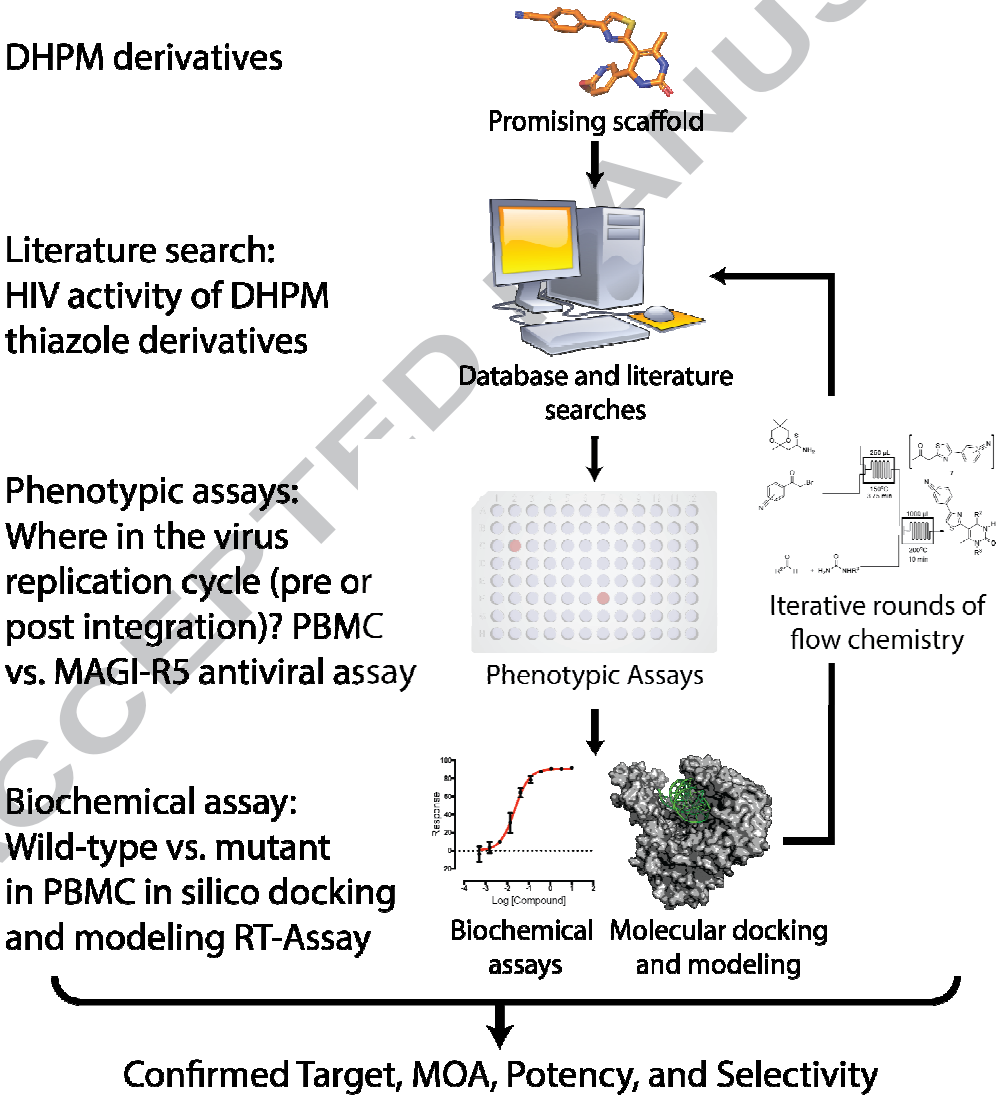

4. Experimental

All reactions were carried out using oven-dried glassware and conducted under a positive pressure of nitrogen unless otherwise specified. NMR spectra were recorded on a JEOL JNM-CS400 (400 MHz) spectrometer. All NMR samples were prepared using DMSO-d_6. High resolution mass spectrometry data were obtained with an Agilent Technologies 6224A time of flight mass spectrometer (MS-TOF) using electrospray ionization at the Sanford-Burnham Medical Research Institute (SBMRI). LC/MS analyses were carried out on a Shimadzu LC/MS 2010 Series LC System with a Kromasil 100 5 micron C18 column (50 x 2.1 mmID). Preparative HPLC purifications were achieved using a Shimadzu SCL-10A system using either a Luna 5 micron C18 column (100 x 30 mmID) or a YMC 10 micron C18 column (150 x 20 mmID). Silica gel purifications were accomplished using a CombiFlash R_f system from Teledyne Isco using RediSep R_f pre-packed columns. All reagents as solvents were used as received from standard suppliers. Microfluidic experiments were conducted using a Syrris AFRICA® synthesis station.

4.1. General Procedure for the Continuous Flow Synthesis of DHPMs. All reactions were conducted in DMF under a positive back pressure of nitrogen at approximately 6.0 bar. Streams of the ketal-protected thioamide **3** (32.5 μL/min, 0.45 M or 0.75 M, DMF, 1 equiv) and a solution of α-bromoketones **4** (32.5 μL/min, 0.45 M or 0.75 M, DMF, 1 equiv) were mixed in a 250 μL glass reactor heated to 150 °C (3.75 min). After exiting the chip, the combined flow (65.0 μL/min) was introduced to a single steam (32.5 μL/min, 0.54 M or 0.9 M, DMF, 1.2 equiv) of aldehydes **5** and ureas **6** in a 1000 μL glass reactor heated to 200 °C (10 min). The reaction flow was then collected (1250 μL) after passing through the back pressure regulator. Once cooled, the crude reaction mixtures were purified using reverse-phase preparative HPLC,

lyophilized, and tested for anti-HIV activity. When measuring the efficiency of the process, the crude reaction mixtures were adsorbed onto silica gel, loaded onto a pre-packed silica gel column (12 g), and chromatographed using either hexanes:EtOAc or CH_2Cl_2:MeOH.

The flow synthesis and characterization of dihydropyrimidine derivatives **1a-d**, **1f**, **1h**, **1j**, and **1k** was reported previously.[10]

4.1.1. Compound characterization data

4.1.1.1. 5-(4-(4-Chlorophenyl)thiazol-2-yl)-4-(3-hydroxyphenyl)-6-methyl-3,4-dihydropyrimidin-2(1*H*)-one (1g). 60 mg (48%). ^{1}H NMR (400 MHz, DMSO-d_6): δ (ppm) 9.07 (d, *J* = 1.4 Hz, 1H), 8.17 (s, 1H), 8.09 (d, *J* = 8.7 Hz, 2H), 7.88 (d, *J* = 8.7 Hz, 2H), 7.70 (m, 1H), 7.25 (d, *J* = 8.7 Hz, 2H), 6.84 (d, *J* = 8.7 Hz, 2H), 5.45 (d, *J* = 2.8 Hz, 1H), 2.36 (s, 3H). ^{13}C NMR (100 MHz, DMSO-d_6): δ (ppm) 165.1, 158.6, 152.3, 151.3, 138.5, 138.3, 136.0, 132.9, 128.0, 126.6, 118.9, 115.1, 113.8, 110.0, 103.9, 56.1, 18.0, one hidden carbon. HRMS (ESI): *m/z* calcd for $C_{20}H_{17}ClN_3O_2S$ $(M + H)^+$ 398.0725, found $(M + H)^+$ 398.0720.

4.1.1.2. 4-(2-(4-(3-Hydroxyphenyl)-6-methyl-2-oxo-1,2,3,4-tetrahydropyrimidin-5-yl)thiazol-4-yl)benzonitrile (1i). 56 mg (46%). ^{1}H NMR (400 MHz, DMSO-d_6): δ (ppm) 9.37 (s, 1H), 9.08 (d, *J* = 1.8 Hz, 1H), 8.20 (s, 1H), 8.11 (m, 2H), 7.89 (m, 2H), 7.73 (m, 1H), 7.09 (t, *J* = 7.8 Hz, 1H), 6.80 (d, *J* = 7.8 Hz, 1H), 6.77 (m, 1H), 6.60 (m, 1H), 5.43 (d, *J* = 3.2 Hz, 1H), 2.38 (s, 3H). ^{13}C NMR (100 MHz, DMSO-d_6): δ (ppm) 165.1, 157.4, 152.3, 151.4, 145.3, 138.6, 138.3, 132.8, 129.4, 126.6, 118.9, 117.5, 115.1, 114.5, 113.5, 110.0, 103.7, 56.6, 18.1. HRMS (ESI): *m/z* calcd for $C_{21}H_{17}N_4O_2S$ $(M + H)^+$ 389.1067, found $(M + H)^+$ 389.1055.

4.1.1.3. 4-(2-(4-(4-Hydroxyphenyl)-6-methyl-2-oxo-1,2,3,4-tetrahydropyrimidin-5-yl)thiazol-4-yl)benzonitrile (1l). 16 mg (22%). ^{1}H NMR (400 MHz, DMSO-d_6): δ (ppm) 9.34 (s, 1H), 9.03 (d, J = 1.8 Hz, 1H), 8.16 (s, 1H), 8.09 (d, J = 8.7 Hz, 2H), 7.88 (d, J = 8.7 Hz, 2H), 7.65 (m, 1H), 7.14 (d, J = 8.2 Hz, 2H), 6.66 (d, J = 8.7 Hz, 2H), 5.36 (d, J = 3.2 Hz, 1H), 2.36 (s, 3H). ^{13}C NMR (100 MHz, DMSO-d_6): δ (ppm) 165.3, 156.8, 152.2, 151.3, 138.3, 138.3, 134.3, 132.8, 128.0, 126.6, 118.9, 115.1, 115.0, 110.0, 103.9, 56.3, 18.0. HRMS (ESI): *m/z* calcd for $C_{21}H_{17}N_4O_2S$ $(M + H)^+$ 389.1067, found $(M + H)^+$ 389.1078.

4.1.1.4. 4-(2-(4-(4-Methoxyphenyl)-6-methyl-2-oxo-1,2,3,4-tetrahydropyrimidin-5-yl)thiazol-4-yl)benzonitrile (1m). 20 mg (27%). ^{1}H NMR (400 MHz, DMSO-d_6): δ (ppm) 9.35 (s, 1H), 9.04 (d, J = 1.4 Hz, 1H), 7.95 (s, 1H), 7.92 (d, J = 8.7 Hz, 2H), 7.70 (m, 1H), 7.47 (d, J = 8.2 Hz, 2H), 7.06 (t, J = 7.9 Hz, 1H), 6.59 (m, 1H), 6.79-6.75 (m, 2H), 5.41 (d, J = 3.7 Hz, 1H), 3.55 (s, 3H), 2.35 (s, 3H). ^{13}C NMR (100 MHz, DMSO-d_6): δ (ppm) 164.7, 157.4, 152.4, 151.9, 145.4, 138.1, 133.0, 132.4, 129.4, 128.8, 127.7, 117.5, 114.4, 113.5, 112.4, 103.9, 66.3, 56.6, 18.0. HRMS (ESI): *m/z* calcd for $C_{22}H_{19}N_4O_2S$ $(M + H)^+$ 403.1223, found $(M + H)^+$ 403.1201.

4.1.1.5. 4-(2-(4-(3-Methoxyphenyl)-6-methyl-2-oxo-1,2,3,4-tetrahydropyrimidin-5-yl)thiazol-4-yl)benzonitrile (1n). 26 mg (35%). ^{1}H NMR (400 MHz, DMSO-d_6): δ (ppm) 9.11 (d, J = 1.8 Hz, 1H), 8.19 (s, 1H), 8.10 (d, J = 8.7 Hz, 2H), 7.88 (d, J = 8.7 Hz, 2H), 7.77 (m, 1H), 7.21 (t, J = 8.2 Hz, 1H), 6.93-6.91 (m, 2H), 6.79 (m, 1H), 5.52 (d, J = 3.2 Hz, 1H), 3.67 (s, 3H), 2.36 (s, 3H). ^{13}C NMR (100 MHz, DMSO-d_6): δ (ppm) 164.9, 159.2, 152.4, 151.3, 145.5, 138.8, 138.2, 132.8, 129.7, 126.6, 118.9, 118.7, 115.2, 113.0, 112.4, 110.1, 103.7, 66.3, 56.4, 18.0. HRMS (ESI): *m/z* calcd for $C_{22}H_{19}N_4O_2S$ $(M + H)^+$ 403.1223, found $(M + H)^+$ 403.1307.

4.1.1.6. 4-(2-(4-(3-Hydroxy-4-methoxyphenyl)-6-methyl-2-oxo-1,2,3,4-tetrahydropyrimidin-5-yl)thiazol-4-yl)benzonitrile (1o). 17 mg (22%). ^{1}H NMR (400 MHz, DMSO-d_6): δ (ppm) 9.03 (d, J = 1.8 Hz, 1H), 8.91 (s, 1H), 8.17 (s, 1H), 8.11 (d, J = 8.7 Hz, 2H), 7.88 (d, J = 8.2 Hz, 2H), 7.65 (m, 1H), 6.95 (d, J = 1.8 Hz, 1H), 6.72-6.65 (m, 2H), 5.40 (d, J = 3.2 Hz, 1H), 3.67 (s, 3H), 2.36 (s, 3H). ^{13}C NMR (100 MHz, DMSO-d_6): δ (ppm) 165.2, 152.3, 151.3, 147.3, 146.0, 138.4, 138.3, 134.9, 132.8, 126.6, 118.9, 118.8, 115.3, 115.1, 111.5, 110.0, 103.8, 56.4, 55.5, 18.0. HRMS (ESI): *m/z* calcd for $C_{22}H_{19}N_4O_3S$ $(M + H)^+$ 419.1172, found $(M + H)^+$ 419.1180.

4.1.1.7. 4-(2-(6-Methyl-2-oxo-4-(4-phenoxyphenyl)-1,2,3,4-tetrahydropyrimidin-5-yl)thiazol-4-yl)benzonitrile (1p). 29 mg (33%). ^{1}H NMR (400 MHz, DMSO-d_6): δ (ppm) 9.12 (d, J = 1.8 Hz, 1H), 8.19 (s, 1H), 8.09 (d, J = 8.2 Hz, 2H), 7.87 (d, J = 8.7 Hz, 2H), 7.78 (m, 1H), 7.37-7.31 (m, 4H), 7.10 (m, 1H), 6.94 (m, 4H), 5.52 (d, J = 3.2 Hz, 1H), 2.37 (s, 3H). ^{13}C NMR (100 MHz, DMSO-d_6): δ (ppm) 164.9, 156.5, 156.0, 152.3, 151.4, 139.0, 138.8, 138.2, 132.9, 130.0, 128.5, 126.6, 123.5, 118.9, 118.6, 118.5, 115.2, 110.0, 103.8, 56.0, 18.1. HRMS (ESI): *m/z* calcd for $C_{27}H_{21}N_4O_2S$ $(M + H)^+$ 465.1380, found $(M + H)^+$ 465.1382.

4.1.1.8. 4-(2-(4-(4-(Benzyloxy)phenyl)-6-methyl-2-oxo-1,2,3,4-tetrahydropyrimidin-5-yl)thiazol-4-yl)benzonitrile (1q). 27 mg (30%). ^{1}H NMR (400 MHz, DMSO-d_6): δ (ppm) 9.08 (d, J = 1.8 Hz, 1H), 8.16 (s, 1H), 8.08 (d, J = 8.7 Hz, 2H), 7.87 (d, J = 8.7 Hz, 2H), 7.71 (m, 1H), 7.39-7.25 (m, 7H), 6.92 (d, J = 8.7 Hz, 2H), 5.45 (d, J = 3.2 Hz, 1H), 5.02 (s, 2H), 2.36 (s, 3H). ^{13}C NMR (100 MHz, DMSO-d_6): δ (ppm) 165.1, 157.7, 152.3, 151.3, 138.5, 138.3, 137.0, 136.3,

132.8, 128.4, 128.0, 127.8, 127.6, 126.6, 118.9, 115.1, 114.7, 110.0, 103.9, 69.1, 56.1, 18.0. HRMS (ESI): *m/z* calcd for $C_{28}H_{23}N_4O_2S$ $(M + H)^+$ 479.1536, found $(M + H)^+$ 479.1537.

4.1.1.9. 4-(2-(6-Methyl-2-oxo-4-(4-(trifluoromethoxy)phenyl)-1,2,3,4-tetrahydropyrimidin-5-yl)thiazol-4-yl)benzonitrile (1r). 34 mg (40%). ^{1}H NMR (400 MHz, DMSO-d_6): δ (ppm) 9.18 (d, *J* = 1.8 Hz, 1H), 8.20 (s, 1H), 8.08 (d, *J* = 8.7 Hz, 2H), 7.87 (d, *J* = 8.7 Hz, 2H), 7.84 (m, 1H), 7.47 (d, *J* = 8.7 Hz, 2H), 7.31 (d, *J* = 8.2 Hz, 2H), 5.61 (d, *J* = 3.2 Hz, 1H), 2.35 (s, 3H). ^{13}C NMR (100 MHz, DMSO-d_6): δ (ppm) 164.6, 152.2, 151.3, 147.5, 143.4, 139.1, 138.2, 132.9, 128.7, 126.6, 121.1, 118.9, 115.3, 110.1, 103.6, 55.8, 18.1. HRMS (ESI): *m/z* calcd for $C_{22}H_{16}F_3N_4O_2S$ $(M + H)^+$ 457.0941, found $(M + H)^+$ 457.0934.

4.1.1.10. 4-(2-(6-Methyl-2-oxo-4-(3-(trifluoromethoxy)phenyl)-1,2,3,4-tetrahydropyrimidin-5-yl)thiazol-4-yl)benzonitrile (1s). 39 mg (45%). ^{1}H NMR (400 MHz, DMSO-d_6): δ (ppm) 9.21 (s, 1H), 8.22 (s, 1H), 8.09 (d, *J* = 8.2 Hz, 2H), 7.88 (m, 3H), 7.45 (t, *J* = 8.0 Hz, 1H), 7.38 (d, *J* = 7.8 Hz, 1H), 7.33 (s, 1H), 7.22 (d, *J* = 7.8 Hz, 1H), 5.66 (d, *J* = 3.2 Hz, 1H), 2.35 (s, 3H). ^{13}C NMR (100 MHz, DMSO-d_6): δ (ppm) 164.4, 152.2, 151.2, 148.3, 146.8, 139.3, 138.1, 132.8, 130.6, 126.6, 125.5, 119.9, 119.2, 118.9, 115.4, 110.1, 103.6, 55.9, 18.0. HRMS (ESI): *m/z* calcd for $C_{22}H_{16}F_3N_4O_2S$ $(M + H)^+$ 457.0941, found $(M + H)^+$ 457.0946.

4.1.1.11. 3-(2-(4-(4-Hydroxyphenyl)-6-methyl-2-oxo-1,2,3,4-tetrahydropyrimidin-5-yl)thiazol-4-yl)benzonitrile (1t). 20 mg (27%). ^{1}H NMR (400 MHz, DMSO-d_6): δ (ppm) 9.35 (s, 1H), 9.04 (d, *J* = 1.8 Hz, 1H), 8.33 (t, *J* = 1.4 Hz, 1H), 8.24 (m, 1H), 8.11 (s, 1H), 7.77 (m, 1H), 7.66-7.62 (m, 2H), 7.15 (d, *J* = 8.7 Hz, 2H), 6.68 (d, *J* = 8.2 Hz, 2H), 5.38 (d, *J* = 2.8 Hz,

1H), 2.37 (s, 3H). ^{13}C NMR (100 MHz, DMSO-d_6): δ (ppm) 165.2, 156.8, 152.2, 151.0, 138.2, 135.3, 134.4, 131.3, 130.5, 130.1, 129.3, 128.0, 118.8, 115.1, 113.7, 111.9, 103.9, 56.3, 18.0. HRMS (ESI): *m/z* calcd for $C_{21}H_{17}N_4O_2S$ $(M + H)^+$ 389.1067, found $(M + H)^+$ 389.1061.

4.1.1.12. 3-(2-(4-(3-Hydroxyphenyl)-6-methyl-2-oxo-1,2,3,4-tetrahydropyrimidin-5-yl)thiazol-4-yl)benzonitrile (1u). 19 mg (26%). ^{1}H NMR (400 MHz, DMSO-d_6): δ (ppm) 9.36 (s, 1H), 9.07 (d, *J* = 1.4 Hz, 1H), 8.33 (d, *J* = 1.4 Hz, 1H), 8.24 (d, *J* = 8.2 Hz, 1H), 8.13 (s, 1H), 7.77 (d, *J* = 7.8 Hz, 1H), 7.70 (m, 1H), 7.63 (t, *J* = 7.8 Hz, 1H), 7.07 (t, *J* = 7.8 Hz, 1H), 6.80-6.75 (m, 2H), 6.59 (dd, *J* = 8.2, 2.3 Hz, 1H), 5.42 (d, *J* = 3.2 Hz, 1H), 2.36 (s, 3H). ^{13}C NMR (100 MHz, DMSO-d_6): δ (ppm) 165.0, 157.4, 152.3, 151.0, 145.3, 138.4, 135.2, 131.3, 130.5, 130.1, 129.4, 129.3, 118.8, 117.5, 114.4, 113.8, 113.5, 111.9, 66.3, 56.6, 18.0. HRMS (ESI): *m/z* calcd for $C_{21}H_{17}N_4O_2S$ $(M + H)^+$ 389.1067, found $(M + H)^+$ 389.1058.

4.1.1.13. 3-(2-(4-(3-Hydroxyphenyl)-1,6-dimethyl-2-oxo-1,2,3,4-tetrahydropyrimidin-5-yl)thiazol-4-yl)benzonitrile (1v). 26 mg (35%). ^{1}H NMR (400 MHz, DMSO-d_6): δ (ppm) 9.39 (s, 1H), 8.37 (t, *J* = 1.4 Hz, 1H), 8.27 (m, 1H), 8.21 (s, 1H), 7.90 (d, *J* = 3.7 Hz, 1H), 7.80 (m, 1H), 7.66 (t, *J* = 7.8 Hz, 1H), 7.08 (t, *J* = 7.8 Hz, 1H), 6.73-6.71 (m, 2H), 6.61 (m, 1H), 5.35 (d, *J* = 3.7 Hz, 1H), 3.17 (s, 3H), 2.56 (s, 3H). ^{13}C NMR (100 MHz, DMSO-d_6): δ (ppm) 165.8, 157.5, 153.4, 151.2, 144.4, 140.3, 135.1, 131.4, 130.5, 130.2, 129.5, 129.3, 118.7, 117.1, 114.5, 113.4, 112.0, 106.7, 55.9, 30.0, 16.6. HRMS (ESI): *m/z* calcd for $C_{22}H_{19}N_4O_2S$ $(M + H)^+$ 403.1223, found $(M + H)^+$ 403.1212.

4.1.1.14. 4-(2-(4-(3-Hydroxyphenyl)-1,6-dimethyl-2-oxo-1,2,3,4-tetrahydropyrimidin-5-yl)thiazol-4-yl)benzonitrile (1w). 21 mg (28%). ^{1}H NMR (400 MHz, DMSO-d_6): δ (ppm) 9.38 (s, 1H), 8.26 (s, 1H), 8.12 (d, *J* = 8.7 Hz, 2H), 7.91-7.89 (m, 3H), 7.07 (t, *J* = 7.8 Hz, 1H), 6.72-6.70 (m, 2H), 6.60 (m, 1H), 5.34 (d, *J* = 3.7 Hz, 1H), 3.16 (s, 3H), 2.56 (s, 3H). ^{13}C NMR (100 MHz, DMSO-d_6): δ (ppm) 165.9, 157.4, 153.3, 151.6, 144.4, 140.5, 138.2, 132.9, 129.5, 126.6, 118.9, 117.1, 115.8, 114.5, 113.3, 110.1, 106.7, 55.8, 30.0, 16.6. HRMS (ESI): *m/z* calcd for $C_{22}H_{19}N_4O_2S$ $(M + H)^+$ 403.1223, found $(M + H)^+$ 403.1216.

4.1.1.15. 4-(2-(6-Methyl-2-oxo-4-(pyridin-2-yl)-1,2,3,4-tetrahydropyrimidin-5-yl)thiazol-4-yl)benzonitrile (1x). 24 mg (34%). ^{1}H NMR (400 MHz, DMSO-d_6): δ (ppm) 9.03 (d, *J* = 1.8 Hz, 1H), 8.46 (m, 1H), 8.14 (s, 1H), 8.06-8.04 (m, 2H), 7.85-7.83 (m, 2H), 7.70-7.65 (m, 2H), 7.35 (d, *J* = 7.8 Hz, 1H), 7.19 (m, 1H), 5.56 (d, *J* = 3.2 Hz, 1H), 2.29 (s, 3H). ^{13}C NMR (100 MHz, DMSO-d_6): δ (ppm) 164.9, 161.9, 152.5, 151.3, 149.3, 139.3, 138.3, 136.8, 132.9, 126.6, 122.8, 121.4, 118.9, 115.0, 110.0, 103.0, 58.4, 18.2. HRMS (ESI): *m/z* calcd for $C_{20}H_{16}N_5OS$ $(M + H)^+$ 374.1070, found $(M + H)^+$ 374.1063.

4.1.1.16. 4-(2-(6-Methyl-2-oxo-4-(pyridin-3-yl)-1,2,3,4-tetrahydropyrimidin-5-yl)thiazol-4-yl)benzonitrile (1y). 27 mg (39%). ^{1}H NMR (400 MHz, DMSO-d_6): δ (ppm) 9.22 (d, *J* = 1.8 Hz, 1H), 8.59 (d, *J* = 2.3 Hz, 1H), 8.42 (dd, *J* = 4.6, 1.4 Hz, 1H), 8.22 (s, 1H), 8.09-8.07 (m, 2H), 7.90-7.85 (m, 3H), 7.72 (m, 1H), 7.34 (dd, *J* = 7.8, 4.6 Hz, 1H), 5.67 (d, *J* = 3.2 Hz, 1H), 2.36 (s, 3H). ^{13}C NMR (100 MHz, DMSO-d_6): δ (ppm) 164.2, 159.1, 152.2, 151.3, 148.7, 148.3, 139.4, 139.3, 138.1, 134.3, 132.9, 126.6, 123.9, 118.9, 115.4, 110.1, 103.4, 54.4, 18.0. HRMS (ESI): *m/z* calcd for $C_{20}H_{16}N_5OS$ $(M + H)^+$ 374.1070, found $(M + H)^+$ 374.1061.

4.1.1.17. 4-(2-(6-Methyl-2-oxo-4-(pyridin-4-yl)-1,2,3,4-tetrahydropyrimidin-5-yl)thiazol-4-yl)benzonitrile (1z). 32 mg (46%). ^{1}H NMR (400 MHz, DMSO-d_6): δ (ppm) 9.22 (d, J = 1.8 Hz, 1H), 8.49 (d, J = 5.5 Hz, 1H), 8.23 (s, 1H), 8.09-8.06 (m, 2H), 7.92-7.86 (m, 3H), 7.33 (dd, J = 4.6, 1.4 Hz, 2H), 5.64 (d, J = 3.7 Hz, 1H), 2.33 (s, 3H). HRMS (ESI): *m/z* calcd for $C_{20}H_{16}N_5OS$ $(M + H)^+$ 374.1070, found $(M + H)^+$ 374.1061.

4.1.1.18. 4-(2-(4-(6-Fluoropyridin-3-yl)-6-methyl-2-oxo-1,2,3,4-tetrahydropyrimidin-5-yl)thiazol-4-yl)benzonitrile (1ae). 33 mg (45%). ^{1}H NMR (400 MHz, DMSO-d_6): δ (ppm) 9.24 (d, J = 1.8 Hz, 1H), 8.22 (m, 2H), 8.09-8.06 (m, 2H), 7.93-7.85 (m, 4H), 7.13 (dd, J = 8.5, 2.5 Hz, 1H), 5.70 (d, J = 3.2 Hz, 1H), 2.34 (s, 3H). 164.1, 162.3 (d_{C-F}, J = 234.8 Hz), 152.1, 151.3, 146.0 (d_{C-F}, J = 15.3 Hz), 140.5 (d_{C-F}, J = 8.6 Hz), 139.5, 138.1, 137.9, 132.9, 126.6, 118.9, 115.5, 110.1, 109.8 (d_{C-F}, J = 37.4 Hz), 103.3, 53.5, 18.1. HRMS (ESI): *m/z* calcd for $C_{20}H_{15}FN_5OS$ $(M + H)^+$ 392.0976, found $(M + H)^+$ 392.0989.

4.1.1.19. 4-(2-(4-(5-Fluoropyridin-3-yl)-6-methyl-2-oxo-1,2,3,4-tetrahydropyrimidin-5-yl)thiazol-4-yl)benzonitrile (1af). 47 mg (64%). ^{1}H NMR (400 MHz, DMSO-d_6): δ (ppm) 9.27 (s, 1H), 8.46 (m, 2H), 8.24 (s, 1H), 8.08 (d, J = 8.2 Hz, 2H), 7.92 (s, 1H), 7.88 (d, J = 8.2 Hz, 2H), 7.60 (d, J = 9.6 Hz, 1H), 5.76 (d, J = 2.8 Hz, 1H), 2.36 (s, 3H). HRMS (ESI): *m/z* calcd for $C_{20}H_{15}FN_5OS$ $(M + H)^+$ 392.0976, found $(M + H)^+$ 392.0968.

4.1.1.20. 4-(2-(4-(2-Fluoropyridin-3-yl)-6-methyl-2-oxo-1,2,3,4-tetrahydropyrimidin-5-yl)thiazol-4-yl)benzonitrile (1ag). 36 mg (49%). ^{1}H NMR (400 MHz, DMSO-d_6): δ (ppm) 9.26

(d, *J* = 1.4 Hz, 1H), 8.19 (s, 1H), 8.09 (s, 1H), 8.05 (d, *J* = 8.2 Hz, 2H), 7.90-7.85 (m, 4H), 7.29 (m, 1H), 5.85 (d, *J* = 3.2 Hz, 1H), 2.35 (s, 3H). HRMS (ESI): *m/z* calcd for $C_{20}H_{15}FN_5OS$ $(M + H)^+$ 392.0976, found $(M + H)^+$ 392.0986.

4.1.1.21. 4-(2-(4-(3-Fluoropyridin-4-yl)-6-methyl-2-oxo-1,2,3,4-tetrahydropyrimidin-5-yl)thiazol-4-yl)benzonitrile (1ah). 44 mg (59%). ^{1}H NMR (400 MHz, DMSO-d_6): δ (ppm) 9.31 (s, 1H), 8.53 (s, 1H), 8.35 (d, *J* = 5.0 Hz, 1H), 8.21 (s, 1H), 8.04 (d, *J* = 8.2 Hz, 2H), 7.89-7.87 (m, 3H), 7.40 (m, 1H), 5.94 (d, *J* = 2.8 Hz, 1H), 2.35 (s, 3H). HRMS (ESI): *m/z* calcd for $C_{20}H_{15}FN_5OS$ $(M + H)^+$ 392.0976, found $(M + H)^+$ 392.1009.

4.1.1.22. 4-(2-(4-(6-Chloropyridin-3-yl)-6-methyl-2-oxo-1,2,3,4-tetrahydropyrimidin-5-yl)thiazol-4-yl)benzonitrile (1ai). 36 mg (47%). ^{1}H NMR (400 MHz, DMSO-d_6): δ (ppm) 9.27 (d, *J* = 1.8 Hz, 1H), 8.41 (d, *J* = 2.3 Hz, 1H), 8.23 (s, 1H), 8.08 (m, 2H), 7.88 (m, 3H), 7.78 (dd, *J* = 8.2, 2.8 Hz, 1H), 7.47 (d, *J* = 8.2 Hz, 1H), 5.71 (d, *J* = 3.2 Hz, 1H), 2.34 (s, 3H). ^{13}C NMR (100 MHz, DMSO-d_6): δ (ppm) 164.0, 152.1, 151.3, 149.2, 148.5, 139.6, 139.1, 138.1, 132.9, 126.6, 124.6, 123.8, 118.9, 115.5, 110.2, 103.1, 53.6, 18.1. HRMS (ESI): *m/z* calcd for $C_{20}H_{15}ClN_5OS$ $(M + H)^+$ 408.0680, found $(M + H)^+$ 408.0690.

4.1.1.23. 4-(2-(4-(2-Chloropyridin-4-yl)-6-methyl-2-oxo-1,2,3,4-tetrahydropyrimidin-5-yl)thiazol-4-yl)benzonitrile (1ak). 26 mg (38%). ^{1}H NMR (400 MHz, DMSO-d_6): δ (ppm) 9.30 (d, *J* = 1.8 Hz, 1H), 8.35 (d, *J* = 5.0 Hz, 1H), 8.26 (s, 1H), 8.10-8.07 (m, 2H), 7.97 (m, 1H), 7.90-7.87 (m, 2H), 7.45 (d, *J* = 1.4 Hz, 1H), 7.36 (dd, *J* = 5.0, 1.4 Hz, 1H), 5.70 (d, *J* = 3.7 Hz, 1H), 2.34 (s, 3H). ^{13}C NMR (100 MHz, DMSO-d_6): δ (ppm) 164.0, 156.5, 152.2, 151.3, 150.5, 140.1,

138.1, 132.9, 126.7, 122.2, 121.2, 118.9, 115.8, 110.2, 102.7, 55.1, 18.1. HRMS (ESI): *m/z* calcd for $C_{20}H_{15}ClN_5OS$ $(M + H)^+$ 408.0680, found $(M + H)^+$ 408.0675.

4.1.1.24. 4-(2-(4-(2,6-Dichloropyridin-3-yl)-6-methyl-2-oxo-1,2,3,4-tetrahydropyrimidin-5-yl)thiazol-4-yl)benzonitrile (1al). 35 mg (42%). ^{1}H NMR (400 MHz, DMSO-d_6): δ (ppm) 9.33 (d, *J* = 1.4 Hz, 1H), 8.22 (s, 1H), 8.06 (d, *J* = 8.2 Hz, 2H), 7.94 (m, 1H), 7.87 (d, *J* = 8.7 Hz, 2H), 7.84 (d, *J* = 8.2 Hz, 1H), 7.50 (d, *J* = 8.2 Hz, 1H), 6.00 (d, *J* = 2.8 Hz, 1H), 2.48 (s, 3H). ^{13}C NMR (100 MHz, DMSO-d_6): δ (ppm) 163.5, 151.4, 151.2, 147.9, 147.7, 141.1, 140.3, 137.9, 137.0, 132.7, 126.5, 124.5, 118.8, 115.5, 110.1, 101.9, 53.3, 18.1. HRMS (ESI): *m/z* calcd for $C_{20}H_{14}Cl_2N_5OS$ $(M + H)^+$ 442.0291, found $(M + H)^+$ 442.0283.

4.1.1.25. 4-(2-(4-(6-Bromopyridin-3-yl)-6-methyl-2-oxo-1,2,3,4-tetrahydropyrimidin-5-yl)thiazol-4-yl)benzonitrile (1am). 40 mg (47%). ^{1}H NMR (400 MHz, DMSO-d_6): δ (ppm) 9.27 (d, *J* = 1.4 Hz, 1H), 8.40 (d, *J* = 2.3 Hz, 1H), 8.24 (s, 1H), 8.08 (d, *J* = 8.7 Hz, 2H), 7.88 (m, 3H), 7.68 (dd, *J* = 8.2, 2.8 Hz, 1H), 7.61 (d, *J* = 8.2 Hz, 1H), 5.69 (d, *J* = 3.2 Hz, 1H), 2.34 (s, 3H). ^{13}C NMR (100 MHz, DMSO-d_6): δ (ppm) 163.9, 152.0, 151.2, 149.1, 140.2, 139.6, 139.4, 138.1, 137.8, 132.9, 128.3, 126.6, 118.9, 115.5, 110.1, 103.0, 53.6, 18.1. HRMS (ESI): *m/z* calcd for $C_{20}H_{15}BrN_5OS$ $(M + H)^+$ 454.0156, found $(M + H)^+$ 454.0158.

4.1.1.26. 4-(2-(6-Methyl-2-oxo-4-(6-(trifluoromethyl)pyridin-3-yl)-1,2,3,4-tetrahydropyrimidin-5-yl)thiazol-4-yl)benzonitrile (1ar). 45 mg (54%). ^{1}H NMR (400 MHz, DMSO-d_6): δ (ppm) 9.32 (d, *J* = 1.4 Hz, 1H), 8.79 (d, *J* = 1.8 Hz, 1H), 8.23 (s, 1H), 8.07 (d, *J* = 8.7 Hz, 2H), 8.00 (dd, *J* = 8.0, 2.1 Hz, 1H), 7.95 (m, 1H), 7.87 (d, *J* = 7.9 Hz, 3H), 5.83 (d, *J* =

3.2 Hz, 1H), 2.34 (s, 3H). ^{13}C NMR (100 MHz, DMSO-d_6): δ (ppm) 163.8, 152.0, 151.2, 148.9, 143.4, 139.9, 138.0, 136.3, 132.3, 126.6, 121.1, 118.9, 115.6, 110.2, 102.9, 53.9, 18.1. HRMS (ESI): *m/z* calcd for $C_{21}H_{15}F_3N_5OS$ $(M + H)^+$ 442.0944, found $(M + H)^+$ 442.0932.

4.2. General procedure for the Batch-Mode Synthesis of DHPMs. Reaction mixtures of ketal-protected thioamide **3** (50 mg, 0.246 mmol, 1 equiv) and α-bromoketones **4** (0.246 mmol) were prepared in 0.6 mL of DMF and heated to 150 °C for 5 min in sealed vials. After cooling, aldehydes **5** (0.295 mmol, 1.2 equiv) and ureas **6** (0.295 mmol, 1.2 equiv) were added and the reaction mixtures heated to 200 °C for an additional 10 min. Once cooled, the crude reaction mixtures were purified using reverse-phase preparative HPLC, lyophilized, and tested for anti-HIV activity. When measuring the efficiency of the process, the crude reaction mixtures were adsorbed onto silica gel, loaded onto a pre-packed silica gel column (12 g), and chromatographed using either hexanes:EtOAc or CH_2Cl_2:MeOH.

4.2.1. Compound characterization data

4.2.1.1. 4-(3-Hydroxyphenyl)-6-methyl-5-(4-(4-(trifluoromethyl)phenyl)thiazol-2-yl)-3,4-dihydropyrimidin-2(1*H*)-one (1e). 65 mg (61%). ^{1}H NMR (400 MHz, DMSO-d_6): δ (ppm) 9.37 (s, 1H), 9.08 (d, *J* = 1.4 Hz, 1H), 8.13 (s, 1H), 8.13 (d, *J* = 8.2 Hz, 2H), 7.78 (d, *J* = 8.2 Hz, 2H), 7.74 (m, 1H), 7.08 (t, *J* = 7.8 Hz, 1H), 6.80 (d, *J* = 7.8 Hz, 1H), 6.78 (m, 1H), 6.60 (m, 1H), 5.45 (d, *J* = 3.2 Hz, 1H), 2.37 (s, 3H). ^{13}C NMR (100 MHz, DMSO-d_6): δ (ppm) 165.0, 157.4, 152.4, 151.6, 145.4, 138.4, 137.9, 129.4, 127.9 (q_{C-F}, *J* = 32.6 Hz) 126.5, 125.7, 123.0, 117.5, 114.4,

114.3, 113.5, 103.9, 56.6, 18.0. HRMS (ESI): *m/z* calcd for $C_{21}H_{17}F_3N_3O_2S$ $(M + H)^+$ 432.0988, found $(M + H)^+$ 432.0978.

4.2.1.2. 4-(2-(6-Methyl-2-oxo-4-(quinolin-2-yl)-1,2,3,4-tetrahydropyrimidin-5-yl)thiazol-4-yl)benzonitrile (1aa). 40 mg (51%). ^{1}H NMR (400 MHz, DMSO-d_6): δ (ppm) 9.29 (d, *J* = 1.4 Hz, 1H), 8.81 (d, *J* = 4.6 Hz, 1H), 8.59 (d, *J* = 7.8 Hz, 1H), 8.10 (s, 1H), 8.02 (dd, *J* = 8.2, 0.9 Hz, 1H), 7.95 (m, 1H), 7.81-7.69 (m, 6H), 7.44 (d, *J* = 4.6 Hz, 1H), 6.51 (d, *J* = 3.2 Hz, 1H), 2.44 (s, 3H). ^{13}C NMR (100 MHz, DMSO-d_6): δ (ppm) 164.0, 159.1, 151.7, 150.8, 149.1, 148.1, 139.9, 137.9, 132.5, 129.5, 129.4, 126.6, 126.4, 125.5, 124.3, 118.8, 115.3, 110.0, 103.1, 51.4, 18.1. HRMS (ESI): *m/z* calcd for $C_{24}H_{18}N_5OS$ $(M + H)^+$ 424.1227, found $(M + H)^+$ 424.1226.

4.2.1.3. 4-(2-(6-Methyl-2-oxo-4-(quinolin-4-yl)-1,2,3,4-tetrahydropyrimidin-5-yl)thiazol-4-yl)benzonitrile (1ab). 58 mg (56%). ^{1}H NMR (400 MHz, DMSO-d_6): δ (ppm) 9.19 (d, *J* = 1.8 Hz, 1H), 8.32 (d, *J* = 8.2 Hz, 1H), 8.17 (s, 1H), 8.10-8.07 (m, 2H), 7.98 (d, *J* = 7.3 Hz, 1H), 7.91-7.85 (m, 4H), 7.74 (ddd, *J* = 8.5, 7.0, 1.5 Hz, 1H), 7.58-7.54 (m, 2H), 5.78 (d, *J* = 2.8 Hz, 1H), 2.38 (s, 3H). HRMS (ESI): *m/z* calcd for $C_{24}H_{18}N_5OS$ $(M + H)^+$ 424.1227, found $(M + H)^+$ 424.1211.

4.2.1.4. 4-(2-(4-(1*H*-Indol-2-yl)-6-methyl-2-oxo-1,2,3,4-tetrahydropyrimidin-5-yl)thiazol-4-yl)benzonitrile (1ac). 38 mg (38%). ^{1}H NMR (400 MHz, DMSO-d_6): δ (ppm) 10.78 (s, 1H), 9.16 (d, *J* = 1.8 Hz, 1H), 8.18 (s, 1H), 8.11-8.08 (m, 2H), 7.87-7.85 (m, 2H), 7.68 (m, 1H), 7.40 (d, *J* = 7.8 Hz, 1H), 7.33 (d, *J* = 7.8 Hz, 1H), 7.00 (ddd, *J* = 8.0, 7.0, 1.0 Hz, 1H), 6.90 (m, 1H), 6.23 (d, *J* = 2.3 Hz, 1H), 5.74 (d, *J* = 3.2 Hz, 1H), 2.39 (s, 3H). ^{13}C NMR (100 MHz, DMSO-d_6):

δ (ppm) 165.1, 162.3, 152.4, 151.4, 140.7, 139.3, 138.3, 136.2, 132.8, 127.6, 126.6, 121.0, 119.9, 118.9, 115.1, 111.5, 110.0, 102.1, 99.0. HRMS (ESI): *m/z* calcd for $C_{23}H_{18}N_5OS$ $(M + H)^+$ 412.1227, found $(M + H)^+$ 412.1227.

4.2.1.5. 4-(2-(6-Methyl-4-(1-methyl-1*H*-indol-2-yl)-2-oxo-1,2,3,4-tetrahydropyrimidin-5-yl)thiazol-4-yl)benzonitrile (1ad). 21 mg (20%). ^{1}H NMR (400 MHz, DMSO-d_6): δ (ppm) 9.21 (d, *J* = 1.4 Hz, 1H), 8.15 (s, 1H), 8.05-8.03 (m, 2H), 7.92 (m, 1H), 7.86-7.84 (m, 2H), 7.44 (d, *J* = 8.2 Hz, 1H), 7.40 (d, *J* = 7.8 Hz, 1H), 7.08 (ddd, *J* = 8.2, 7.1, 1.1 Hz, 1H), 6.94 (ddd, *J* = 7.8, 6.9, 0.9 Hz, 1H), 6.27 (s, 1H), 5.89 (d, *J* = 3.7 Hz, 1H), 3.91 (s, 3H), 2.39 (s, 3H). ^{13}C NMR (100 MHz, DMSO-d_6): δ (ppm) 164.9, 162.3, 152.2, 151.3, 141.5, 139.2, 138.2, 137.2, 132.8, 126.8, 126.6, 121.2, 120.1, 118.9, 115.2, 110.0, 109.8, 102.6, 99.1, 48.6, 29.6, 18.0. HRMS (ESI): *m/z* calcd for $C_{24}H_{20}N_5OS$ $(M + H)^+$ 426.1383, found $(M + H)^+$ 426.1367.

4.2.1.6. 4-(2-(4-(2-Chloropyridin-3-yl)-6-methyl-2-oxo-1,2,3,4-tetrahydropyrimidin-5-yl)thiazol-4-yl)benzonitrile (1aj). 54 mg (54%). ^{1}H NMR (400 MHz, DMSO-d_6): δ (ppm) 9.27 (d, *J* = 1.4 Hz, 1H), 8.27 (dd, *J* = 4.6, 1.8 Hz, 1H), 8.19 (s, 1H), 8.05 (m, 2H), 7.89 (m, 1H), 7.85 (m, 2H), 7.78 (dd, *J* = 7.6, 2.1 Hz, 1H), 7.36 (dd, *J* = 7.8, 4.6 Hz, 1H), 5.99 (d, *J* = 3.2 Hz, 1H), 2.38 (s, 3H). HRMS (ESI): *m/z* calcd for $C_{20}H_{15}ClN_5OS$ $(M + H)^+$ 408.0680, found $(M + H)^+$ 408.0685.

4.2.1.7. 4-(2-(4-(6-Methoxypyridin-3-yl)-6-methyl-2-oxo-1,2,3,4-tetrahydropyrimidin-5-yl)thiazol-4-yl)benzonitrile (1an). 48 mg (48%). ^{1}H NMR (400 MHz, DMSO-d_6): δ (ppm) 9.17 (d, *J* = 1.8 Hz, 1H), 8.21 (s, 1H), 8.12 (d, *J* = 2.3 Hz, 1H), 8.11-8.08 (m, 2H), 7.90-7.87 (m, 2H),

7.77 (m, 1H), 7.64 (dd, *J* = 8.5, 2.5 Hz, 1H), 6.77 (d, *J* = 8.2 Hz, 1H), 5.58 (d, *J* = 2.8 Hz, 1H), 3.77 (s, 3H), 2.36 (s, 3H). ^{13}C NMR (100 MHz, DMSO-d_6): δ (ppm) 164.5, 163.0, 152.2, 151.3, 145.1, 139.0, 138.2, 137.7, 132.9, 132.6, 126.6, 118.9, 115.3, 110.7, 110.1, 103.5, 53.8, 53.1, 18.0. HRMS (ESI): *m/z* calcd for $C_{21}H_{18}N_5O_2S$ $(M + H)^+$ 404.1176, found $(M + H)^+$ 404.1165.

4.2.1.8. 4-(2-(4-(5-Methoxypyridin-3-yl)-6-methyl-2-oxo-1,2,3,4-tetrahydropyrimidin-5-yl)thiazol-4-yl)benzonitrile (1ao). 60 mg (48%). ^{1}H NMR (400 MHz, DMSO-d_6): δ (ppm) 9.21 (d, *J* = 1.8 Hz, 1H), 8.21 (s, 1H), 8.17 (s, 1H), 8.15 (d, *J* = 2.8 Hz, 1H), 8.11-8.08 (m, 2H), 7.89-7.85 (m, 3H), 7.28 (m, 1H), 5.67 (d, *J* = 3.2 Hz, 1H), 3.76 (s, 3H), 2.35 (s, 3H). ^{13}C NMR (100 MHz, DMSO-d_6): δ (ppm) 164.3, 155.4, 152.3, 151.3, 140.4, 140.3, 139.4, 138.2, 135.9, 132.9, 126.6, 119.3, 118.9, 115.5, 110.2, 103.3, 55.6, 54.3, 18.1. HRMS (ESI): *m/z* calcd for $C_{21}H_{18}N_5O_2S$ $(M + H)^+$ 404.1176, found $(M + H)^+$ 404.1165.

4.2.1.9. 4-(2-(4-(2-Methoxypyridin-3-yl)-6-methyl-2-oxo-1,2,3,4-tetrahydropyrimidin-5-yl)thiazol-4-yl)benzonitrile (1ap). 56 mg (57%). ^{1}H NMR (400 MHz, DMSO-d_6): δ (ppm) 9.12 (d, *J* = 1.4 Hz, 1H), 8.15 (s, 1H), 8.05-8.02 (m, 3H), 7.88-7.86 (m, 2H), 7.55 (m, 1H), 7.51 (dd, *J* = 7.3, 1.8 Hz, 1H), 6.89 (dd, *J* = 7.3, 4.6 Hz, 1H), 5.79 (d, *J* = 3.2 Hz, 1H), 3.94 (s, 3H), 2.39 (s, 3H). ^{13}C NMR (100 MHz, DMSO-d_6): δ (ppm) 164.5, 160.7, 152.2, 151.3, 145.9, 139.7, 138.2, 136.2, 132.8, 126.5, 125.4, 118.9, 117.2, 115.0, 110.0, 101.9, 53.4, 51.0, 18.0. HRMS (ESI): *m/z* calcd for $C_{21}H_{18}N_5O_2S$ $(M + H)^+$ 404.1176, found $(M + H)^+$ 404.1161.

4.2.1.10. 4-(2-(4-(6-Methoxypyridin-2-yl)-6-methyl-2-oxo-1,2,3,4-tetrahydropyrimidin-5-yl)thiazol-4-yl)benzonitrile (1aq). 37 mg (37%). ^{1}H NMR (400 MHz, DMSO-d_6): δ (ppm) 9.10

(d, *J* = 1.4 Hz, 1H), 8.19 (s, 1H), 8.12-8.10 (m, 2H), 7.89-7.87 (m, 2H), 7.64 (s, 1H), 7.60 (dd, *J* = 7.3, 7.3 Hz, 1H), 6.94 (d, *J* = 6.9 Hz, 1H), 6.63 (d, *J* = 7.8 Hz, 1H), 5.51 (d, *J* = 3.2 Hz, 1H), 3.73 (s, 3H), 2.30 (s, 3H). ^{13}C NMR (100 MHz, DMSO-d_6): δ (ppm) 165.2, 163.2, 159.6, 153.3, 151.3, 139.6, 139.2, 138.4, 132.9, 126.6, 119.0, 115.0, 113.4, 110.1, 109.2, 103.2, 57.7, 52.8, 18.1. HRMS (ESI): *m/z* calcd for $C_{21}H_{18}N_5O_2S$ $(M + H)^+$ 404.1176, found $(M + H)^+$ 404.1161.

4.1.1.27. 4-(2-(6-Methyl-2-oxo-4-(6-phenoxypyridin-3-yl)-1,2,3,4-tetrahydropyrimidin-5-yl)thiazol-4-yl)benzonitrile (1as). 29 mg (33%). ^{1}H NMR (400 MHz, DMSO-d_6): δ (ppm) 9.21 (s, 1H), 8.19 (m, 1H), 8.11-8.06 (m, 3H), 7.93 (s, 1H), 7.86 (dd, *J* = 8.5, 2.1 Hz, 2H), 7.82-7.78 (m, 2H), 7.35 (t, *J* = 7.1 Hz, 2H), 7.17 (m, 1H), 7.05 (d, *J* = 8.2 Hz, 2H), 6.98 (d, *J* = 8.2 Hz, 1H), 5.63 (d, *J* = 2.8 Hz, 1H), 2.35 (s, 3H). ^{13}C NMR (100 MHz, DMSO-d_6): δ (ppm) 164.3, 162.5, 162.3, 153.8, 152.2, 151.3, 145.7, 139.3, 138.6, 138.1, 134.6, 132.8, 129.6, 126.6, 124.5, 121.2, 118.9, 115.3, 111.5, 110.1, 103.4, 53.6, 18.0. HRMS (ESI): *m/z* calcd for $C_{26}H_{20}N_5OS$ $(M + H)^+$ 466.1332, found $(M + H)^+$ 466.1340.

4.2.1.11. 4-Acetyl-3-methylphenyl trifluoromethanesulfonate. To a solution of 1-(4-hydroxy-2-methylphenyl)ethan-1-one (67 mmol, 1 equiv) in pyridine (1M) at 0 °C, trifluoromethanesulfonic anhydride (100 mmol, 1.5 equiv) was added. The reaction was allowed to warm to room temperature while stirring overnight. The reaction was quenched by pouring the mixture onto ice-cold water. The aqueous mixture was extracted with diethyl ether, and the organics were washed with water, 1M HCl, water, and then brine. The organic phase was dried over Na_2SO_4 and concentrated *in vacuo.* The crude reaction mixture was adsorbed onto silica gel, loaded onto a pre-packed silica gel column, and chromatographed using hexanes:EtOAc (87%).

4.2.1.12. 4-Acetyl-3-methylbenzonitrile. A solution of 4-acetyl-3-methylphenyl trifluoromethanesulfonate (62 mmol) in anhydrous DMF (0.5M) was degassed with N_2. To this solution $Zn(CN)_2$ (74.4 mmol, 1.2 equiv) and $Pd(PPh_3)_4$ (3.1 mmol, 0.05 equiv) were added and the reaction mixture degassed again. The reaction was heated at 80 °C for 15h. The reaction mixture was dissolved in water and extracted with EtOAc. The organics were washed with brine, dried over Na_2SO_4 and concentrated *in vacuo*. The crude reaction mixture was adsorbed onto silica gel, loaded onto a pre-packed silica gel column, and chromatographed using hexanes:EtOAc (73%).

4.2.1.13. 4-(2-Bromoacetyl)-3-methylbenzonitrile. A solution of 4-acetyl-3-methylbenzonitrile (45 mmol, 1 equiv) in methanol (1M) was chilled to 0 °C. Bromine (45 mmol, 1 equiv) was added drop-wise and the reaction mixture allowed to warm to room temperature as the red color disappeared. At this point, an equal volume of water (45 mL) was added, and the reaction mixture stirred for 15h. The reaction was neutralized with solid $NaHCO_3$ and extracted with diethyl ether. The organics were washed with water, dried over Na_2SO_4 and concentrated *in vacuo*. The crude product mixture was utilized in the next step without further purification.

4.2.1.14. 3-Methyl-4-(2-(6-methyl-4-(1-methyl-1H-indol-2-yl)-2-oxo-1,2,3,4-tetrahydropyrimidin-5-yl)thiazol-4-yl)benzonitrile (1at). A mixture of ketal-protected thioamide **3** (1.67 mmol, 1 equiv) and 4-(2-bromoacetyl)-3-methylbenzonitrile (1.67 mmol, 1 equiv) was heated to 150 °C for 5 min in DMF (0.8M). After cooling, a solution of 1-methyl-1*H*-indole-2-carbaldehyde (2 mmol, 1.2 equiv) and urea (2 mmol, 1.2 equiv) in DMF (0.8 M) was added and the reaction mixture heated to 200 °C for an additional 10 min. Once cooled, the crude

reaction mixture was adsorbed onto silica gel, loaded onto a pre-packed silica gel column, and chromatographed using hexanes:EtOAc. ^{1}H NMR (400 MHz, $(CD_3)_2SO$) δ, ppm: 9.20 (s, 1H), 7.90 (s, 1H), 7.78 (s, 1H), 7.72 (m, 2H), 7.67 (m, 1H), 7.43 (dd, 2H, J = 12, 8 Hz), 7.10 (t, 1H, J = 7 Hz), 6.96 (t, 1H, J = 7 Hz), 6.27 (s, 1H), 5.85 (s, 1H), 3.87 (s, 3H), 2.42 (s, 3H), 2.31 (s, 3H). ^{13}C NMR (400 MHz, $(CD_3)_2SO$) δ, ppm: 175.56, 163.70, 152.20, 151.53, 141.45, 138.89, 138.52, 137.18, 136.99, 134.33, 130.06, 129.58, 126.73, 121.13, 120.08, 119.12, 116.93, 110.10, 109.62, 102.59, 99.08, 48.70, 29.48, 20.48, 17.80. HRMS (ESI): *m/z* calcd for $C_{25}H_{21}N_5OS$ 439.15, found $(M + H)^+$ 440.1531.

4.3. Resolution of (*R*)-1i and (*S*)-1i. Baseline separation of the enantiomers of DHPM **1i** was achieved using the Chiral Cel OD-RH analytical HPLC column (Daicel/Chiral Technologies). First, **1i** (10 mg) was dissolved in DMSO (1 mL) and carefully filtered. Then, each isocratic injection was run using H_2O:CH_3CN (40:60) over 8 min. A flow rate of 0.8 mL/min was used and injection volumes of 40 μL could be reached without compromising baseline separation. After 20 injections, 2.6 mg of each isomer was isolated. Enantiomeric purity of the resolved stereoisomers was confirmed using this same procedure. Absolute configurations were assigned based on the combination of molecular docking studies of each enantiomer with the HIV-1 RT etravirine binding pocket and biochemical assay inhibition results (Table ST2; see Supplementary Data ST2).

4.4. MAGI-CCR5 antiviral assay. MAGI-CCR5 cells (obtained from the NIH AIDS Research and Reference Reagent Program). Cells were seeded at a density of 1 x 10^4 cells/well into a 96-well plate. The following morning, the media was decanted and replenished with compounds

diluted in DMSO and HIV_{Ba-L}, NL4-3 and A17 at an MOI of 10 $TCID_{50}$/mL. Compounds were evaluated at six concentrations (triplicate wells/concentration). Identical uninfected plates were prepared for parallel cytotoxicity testing. The cultures were incubated for 48 hours in an incubator maintained at 37°C and 5% CO_2. Efficacy was assessed by □□galactosidase expression (Gal-screen™; Tropix, Bedford MA) and cytotoxicity by MTS staining (CellTiter Reagent, Promega).

4.5. PBMC assay. Fresh human PBMCs were isolated from screened donors, seronegative for HIV and HBV (Biological Specialty Corporation, Colmar, PA). Blood was processed for PBMC isolation by layered over Ficoll-Hypaque density gradient. Banded PBMCs were collected; washed in PBS and suspended at 1 x 10^6 cells/mL in RPMI 1640 supplemented with 15 % Fetal Bovine Serum (FBS), 2 mM L-glutamine, 100 U/mL penicillin, 100 µg/mL streptomycin, and 4 µg/mL Phytohemagglutinin (PHA; Sigma, St. Louis, MO; catalog #L1668). The cells were incubated for 48-72 hours at 37°C prior to use. After incubation, PBMCs were stimulated with 20 U/mL recombinant human IL-2 (R&D Systems Inc., Minneapolis, MN; catalog #202IL). Monocytes-derived-macrophages were depleted from the culture as the result of adherence to the tissue culture flask. PHA stimulated cells from at least two normal donors were pooled, diluted in fresh medium to a final concentration of 1 x 10^6 cells/mL, and seeded in the interior wells of a 96 well round bottom microplate at 50 µL/well (5 x 10^4 cells/well). For these studies, HIV_{Ba-L} was used at a final concentration of MOI ≅ 0.1/well. Cytotoxicity studies were performed using an MTS end-point (CellTiter Reagent, Promega). The PBMC cultures were maintained for six days following infection in a humidified incubator maintained at 37°C, 5% CO_2. After this

period, cell-free supernatant samples were collected for analysis of reverse transcriptase activity, and compound cytotoxicity was measured by addition of MTS staining.

4.6. RT biochemical assay. The HIV-1 RT (Protease derived) was used in experiments (obtained from the NIH AIDS Research and Reference Reagent Program; provided by Stuart Le Grice and Jennifer T Miller). RT activity was determined by the incorporation of radiolabeled deoxyribonucleotides into the newly synthesized DNA strand. The standard RT reaction mixture contained a synthetic homopolymeric template/primer [poly(rA)/oligo(dT)] or *in vitro* transcribed viral RNA derived from the HIV-1_{NL4-3} 5'-LTR region (nucleotide residues 454 to 652) and a primer complementary to the primer binding site (PBS, nucleotide residues 636 to 652), radiolabeled deoxyribonucleotide, dNTPs and RT. The reaction was carried out in a volume of 40 µl containing 50 mM Tris HCl, pH 7.8, 50 mM KCl, 5mM MgCl2, 1mM DTT, 50 µM each of dATP, dCTP, dGTP, 50 nM dTTP, 1µCi of [^{3}H] dTTP (70-90Ci/mM) and 5 nM template/primer. The reaction was initiated by the addition of 10 nM RT. For compound screening, serially diluted test articles were added to the reaction followed by the addition of RT. The reaction mixture was incubated at 37°C for 1h, then quenched by the addition of ice-cold trichloroacetic acid (TCA) to the final concentration of 10%. The plate was incubated at 4°C for 1h to precipitate the synthesized DNA, then rinsed 3-times with 10% TCA and 1 time with 70% ethanol. After addition of 25 µl scintillation fluid to completely dried wells, radioactivity is counted by MicroBeta scintillation counter.

Compounds were evaluated in triplicate, six-serial dilutions for each experiment. The IC_{50} was calculated using the growth function in excel. Experiments were performed in triplicate and the average IC_{50} and the standard deviation are reported.

4.7. Microsomal stability *in vitro* assay. Pooled rat liver microsomes (BD Biosciences, # 452701) were preincubated with test compounds at 37.5 °C for 5 min in the absence of NADPH. The reaction was initiated by addition of NADPH and incubated under the same conditions. The final incubation concentrations were 4 μM test compound, 2 mM NADPH, and 1 mg/mL (total protein) liver microsomes in phosphate-buffered saline (PBS) at pH 7.4. One aliquot (100 μL) of the incubation mixture was withdrawn at 15 min time points and combined immediately with 100 μL of ACN/MeOH. After mixing, the sample was centrifuged at approximately 13000 rpm for 12 min. The supernatant was filtered and transferred into an autosampler vial and the amount of test compound was quantified using a Shimadzu LCMS 2010EV mass spectrometer. The change of the AUC (area under the curve) of the parent compound as a function of time was used as a measure of microsomal stability. Test compounds were run in duplicate with a positive control.

4.8. Plasma stability *in vitro* assay. A 20 μL aliquot of a 10 mM solution in DMSO of the test compound was added to 2.0 mL of heparinized rat plasma (Lampire, P1-150N) to obtain a 100 μM final solution. The mixture was incubated for 1 h at 37.5 °C. Aliquots of 100 μL were taken at 15 min intervals and diluted with 100 μL of MeOH/ACN. After mixing, the sample was centrifuged at approximately 13000 rpm for 12 min. The supernatant was filtered and transferred into an autosampler vial and the amount of test compound was quantified using the Shimadzu

LCMS-2010EV system. The change of the AUC of the parent compound in function of time was used as a measure of plasma stability.

4.9. Parallel artificial membrane permeation assay (PAMPA). A 96-well microtiter plate (Millipore, # MSSACCEPTOR) was filled with 300 µL aqueous buffer solution (in general phosphate pH 7.2 buffer was used) and covered with a microtiter filterplate (Millipore, # MAIPNTR10) to create a sort of sandwich construction. The hydrophobic filter material was impregnated with a 10% solution of polar brain lipid extract in chloroform (Avanti) as the artificial membrane, and the organic solvent was allowed to completely evaporate. Permeation studies were started by the transfer of 150 µL of a 100 µM test compound solution on top of the filter plate. The maximum DMSO content of the stock solutions was <1.5%. In parallel, an equilibrium solution lacking a membrane was prepared using the exact concentrations and specifications but lacking the membrane. The concentrations of the acceptor and equilibrium solutions were determined using the Shimadzu LCMS-2010EV and AUC methods. The Acceptor plate and equilibrium plate concentrations were used to calculate the permeability rate (Log P_e) of the compounds. The log P_e values were calculated using the following equation:

$$LogP_e = \log\{C \bullet -\ln(1-[Drug]_{Acceptor}/[Drug]_{Equilibrium})\}$$

$$C = (V_D \bullet V_A) / ((V_D + V_A)\ Area \bullet time))$$

In this equation, V_D (cm^3) is the donor volume (0.150 cm^3), V_A (cm^3) is the acceptor volume (0.300 cm^3), Area (cm^2) is the accessible filter area (0.168 cm^2), and time (s) is the incubation time. $[Drug]_{Acceptor}$ and $[Drug]_{Equilibruim}$ are concentration of the test drug for the sample (Acceptor) and reference (Equilibrium) solutions in the acceptor compartment.

Acknowledgements

This work was supported by National Institutes of Health grant nos. AI078048, CA140427, HG005033, GM079590, and GM081261. The HIV-1 RT (Protease derived) was obtained through the NIH AIDS Research and Reference Reagent Program, Division of AIDS, NIAID, NIH (catalog number 3555) from Stuart Le Grice and Jennifer T Miller. The authors would like to thank Marie K Mankowski and Chelsea R Laylock for their technical support.

Supplementary Data

Supplementary data associated with this article can be found, in the online version, at http…

References

1. E.B. Lansdon, K.M. Brendza, M. Hung, R. Wang, S. Mukund, D. Jin, G. Birkus, N. Kutty, X. Liu, *Journal of medicinal chemistry*, **2010**, 53, 4295-4299.
2. V.J. Haupt, M. Schroeder, *Briefings in bioinformatics*, **2011**, 12, 312-326.
3. Y. Hu, E. Lounkine, J. Bajorath, *The AAPS journal*, **2014**, 16, 847-859.
4. Y. Hu, J. Bajorath, *European journal of medicinal chemistry*, **2014**, 76, 427-434.
5. Y. Hu, J. Bajorath, *F1000Research*, **2014**, 3, 218.
6. M. Schenone, V. Dancik, B.K. Wagner, P.A. Clemons, *Nature chemical biology*, **2013**, 9, 232-240.
7. X. Liu, F. Zhu, X.H. Ma, Z. Shi, S.Y. Yang, Y.Q. Wei, Y.Z. Chen, *Current medicinal chemistry*, **2013**, 20, 1646-1661.
8. N.T. Issa, S.W. Byers, S. Dakshanamurthy, *Current topics in medicinal chemistry*, **2013**, 13, 2328-2336.
9. N.T. Issa, J. Kruger, S.W. Byers, S. Dakshanamurthy, *Expert review of clinical pharmacology*, **2013**, 6, 95-97.
10. N. Pagano, A. Herath, N.D.P. Cosford, *J Flow Chem*, **2011**, 1, 28-U63.
11. I.T. Phucho, A. Nongpiur, S. Tumtin, R. Nongrum, R.L. Nongkhlaw, *Rasayan Journal of Chemistry*, **2009**, 2, 662-676.
12. C.O. Kappe, *European journal of medicinal chemistry*, **2000**, 35, 1043-1052.
13. J. Kim, T. Ok, C. Park, W. So, M. Jo, Y. Kim, M. Seo, D. Lee, S. Jo, Y. Ko, I. Choi, Y. Park, J. Yoon, M.K. Ju, J. Ahn, J. Kim, S.J. Han, T.H. Kim, J. Cechetto, J. Nam, M. Liuzzi, P. Sommer, Z. No, *Bioorganic & medicinal chemistry letters*, **2012**, 22, 2522-2526.
14. A.B. Hutchinson, P.G. Farnham, H.D. Dean, D.U. Ekwueme, C. del Rio, L. Kamimoto, S.E. Kellerman, *Journal of acquired immune deficiency syndromes*, **2006**, 43, 451-457.
15. K.A. Gebo, J.A. Fleishman, R. Conviser, J. Hellinger, F.J. Hellinger, J.S. Josephs, P. Keiser, P. Gaist, R.D. Moore, H.I.V.R. Network, *Aids*, **2010**, 24, 2705-2715.
16. NIH, FDA-Approved HIV Medicines, HIV/AIDS Fact Sheets, AIDSinfo, 2014.
17. E.L. Asahchop, M.A. Wainberg, R.D. Sloan, C.L. Tremblay, *Antimicrob Agents Chemother*, **2012**, 56, 5000-5008.
18. M.A. Wainberg, *Scientifica (Cairo)*, **2012**, 2012, 238278.
19. A.J. Japour, D.L. Mayers, V.A. Johnson, D.R. Kuritzkes, L.A. Beckett, J.M. Arduino, J. Lane, R.J. Black, P.S. Reichelderfer, R.T. D'Aquila, et al., *Antimicrob Agents Chemother*, **1993**, 37, 1095-1101.
20. N. Pagano, M.L. Heil, N.D.P. Cosford, *Synthesis-Stuttgart*, **2012**, 44, 2537-2546.
21. L. Di, E.H. Kerns, K. Fan, O.J. McConnell, G.T. Carter, *European journal of medicinal chemistry*, **2003**, 38, 223-232.
22. M.A. Thompson, J.A. Aberg, P. Cahn, J.S. Montaner, G. Rizzardini, A. Telenti, J.M. Gatell, H.F. Gunthard, S.M. Hammer, M.S. Hirsch, D.M. Jacobsen, P. Reiss, D.D. Richman, P.A. Volberding, P. Yeni, R.T. Schooley, A.S.-U.S.A. International, *JAMA : the journal of the American Medical Association*, **2010**, 304, 321-333.
23. R.M. Grant, J.R. Lama, P.L. Anderson, V. McMahan, A.Y. Liu, L. Vargas, P. Goicochea, M. Casapia, J.V. Guanira-Carranza, M.E. Ramirez-Cardich, O. Montoya-Herrera, T. Fernandez, V.G. Veloso, S.P. Buchbinder, S. Chariyalertsak, M. Schechter, L.G. Bekker, K.H. Mayer, E.G. Kallas, K.R. Amico, K. Mulligan, L.R. Bushman, R.J. Hance, C. Ganoza, P. Defechereux, B. Postle, F. Wang, J.J. McConnell, J.H. Zheng, J. Lee, J.F. Rooney, H.S. Jaffe, A.I. Martinez, D.N.

Burns, D.V. Glidden, T. iPrEx Study, *The New England journal of medicine*, **2010**, 363, 2587-2599.
24. C. Centers for Disease, Prevention, *MMWR. Morbidity and mortality weekly report*, **2011**, 60, 65-68.
25. H. Grosskurth, F. Mosha, J. Todd, E. Mwijarubi, A. Klokke, K. Senkoro, P. Mayaud, J. Changalucha, A. Nicoll, G. ka-Gina, et al., *Lancet*, **1995**, 346, 530-536.
26. C. Centers for Disease, Prevention, *MMWR. Morbidity and mortality weekly report*, **2006**, 55, 592-597.
27. E.M. Connor, R.S. Sperling, R. Gelber, P. Kiselev, G. Scott, M.J. O'Sullivan, R. VanDyke, M. Bey, W. Shearer, R.L. Jacobson, et al., *The New England journal of medicine*, **1994**, 331, 1173-1180.
28. Q. Abdool Karim, S.S. Abdool Karim, J.A. Frohlich, A.C. Grobler, C. Baxter, L.E. Mansoor, A.B. Kharsany, S. Sibeko, K.P. Mlisana, Z. Omar, T.N. Gengiah, S. Maarschalk, N. Arulappan, M. Mlotshwa, L. Morris, D. Taylor, C.T. Group, *Science*, **2010**, 329, 1168-1174.
29. M.C. Thigpen, P.M. Kebaabetswe, L.A. Paxton, D.K. Smith, C.E. Rose, T.M. Segolodi, F.L. Henderson, S.R. Pathak, F.A. Soud, K.L. Chillag, R. Mutanhaurwa, L.I. Chirwa, M. Kasonde, D. Abebe, E. Buliva, R.J. Gvetadze, S. Johnson, T. Sukalac, V.T. Thomas, C. Hart, J.A. Johnson, C.K. Malotte, C.W. Hendrix, J.T. Brooks, T.D.F.S. Group, *The New England journal of medicine*, **2012**, 367, 423-434.
30. J.B. Jackson, P. Musoke, T. Fleming, L.A. Guay, D. Bagenda, M. Allen, C. Nakabiito, J. Sherman, P. Bakaki, M. Owor, C. Ducar, M. Deseyve, A. Mwatha, L. Emel, C. Duefield, M. Mirochnick, M.G. Fowler, L. Mofenson, P. Miotti, M. Gigliotti, D. Bray, F. Mmiro, *Lancet*, **2003**, 362, 859-868.
31. G. Kesho Bora Study, I. de Vincenzi, *The Lancet infectious diseases*, **2011**, 11, 171-180.
32. H.M. Coovadia, E.R. Brown, M.G. Fowler, T. Chipato, D. Moodley, K. Manji, P. Musoke, L. Stranix-Chibanda, V. Chetty, W. Fawzi, C. Nakabiito, L. Msweli, R. Kisenge, L. Guay, A. Mwatha, D.J. Lynn, S.H. Eshleman, P. Richardson, K. George, P. Andrew, L.M. Mofenson, S. Zwerski, Y. Maldonado, H.p. team, *Lancet*, **2012**, 379, 221-228.
33. WHO, Use of Antiretroviral Drugs for Treating Pregnant Women and Preventing HIV Infection in Infants, in: WHO (Ed.), World Health Organization, Geneva, Switzerland, 2012, pp. 8.
34. C.S. Chasela, M.G. Hudgens, D.J. Jamieson, D. Kayira, M.C. Hosseinipour, A.P. Kourtis, F. Martinson, G. Tegha, R.J. Knight, Y.I. Ahmed, D.D. Kamwendo, I.F. Hoffman, S.R. Ellington, Z. Kacheche, A. Soko, J.B. Wiener, S.A. Fiscus, P. Kazembe, I.A. Mofolo, M. Chigwenembe, D.S. Sichali, C.M. van der Horst, B.A.N.S. Group, *The New England journal of medicine*, **2010**, 362, 2271-2281.
35. R. Klein, K. Struble, Truvada approved to reduce the risk of sexually transmitted HIV in people who are not infected with the virus., FDA, FDA, 2012.
36. K. Das, J.D. Bauman, A.S. Rim, C. Dharia, A.D. Clark, Jr., M.J. Camarasa, J. Balzarini, E. Arnold, *Journal of medicinal chemistry*, **2011**, 54, 2727-2737.
37. K. Das, A.D. Clark, Jr., P.J. Lewi, J. Heeres, M.R. De Jonge, L.M. Koymans, H.M. Vinkers, F. Daeyaert, D.W. Ludovici, M.J. Kukla, B. De Corte, R.W. Kavash, C.Y. Ho, H. Ye, M.A. Lichtenstein, K. Andries, R. Pauwels, M.P. De Bethune, P.L. Boyer, P. Clark, S.H. Hughes, P.A. Janssen, E. Arnold, *Journal of medicinal chemistry*, **2004**, 47, 2550-2560.
38. P.A. Janssen, P.J. Lewi, E. Arnold, F. Daeyaert, M. de Jonge, J. Heeres, L. Koymans, M. Vinkers, J. Guillemont, E. Pasquier, M. Kukla, D. Ludovici, K. Andries, M.P. de Bethune, R.

Pauwels, K. Das, A.D. Clark, Jr., Y.V. Frenkel, S.H. Hughes, B. Medaer, F. De Knaep, H. Bohets, F. De Clerck, A. Lampo, P. Williams, P. Stoffels, *Journal of medicinal chemistry*, **2005**, 48, 1901-1909.
39. A. Jacobo-Molina, J. Ding, R.G. Nanni, A.D. Clark, Jr., X. Lu, C. Tantillo, R.L. Williams, G. Kamer, A.L. Ferris, P. Clark, et al., *Proceedings of the National Academy of Sciences of the United States of America*, **1993**, 90, 6320-6324.
40. L.A. Kohlstaedt, J. Wang, J.M. Friedman, P.A. Rice, T.A. Steitz, *Science*, **1992**, 256, 1783-1790.
41. K. Das, P.J. Lewi, S.H. Hughes, E. Arnold, *Progress in biophysics and molecular biology*, **2005**, 88, 209-231.
42. V.A. Braz, M.D. Barkley, R.A. Jockusch, P.L. Wintrode, *Biochemistry*, **2010**, 49, 10565-10573.
43. K.A. Paris, O. Haq, A.K. Felts, K. Das, E. Arnold, R.M. Levy, *Journal of medicinal chemistry*, **2009**, 52, 6413-6420.
44. K. Das, S.E. Martinez, J.D. Bauman, E. Arnold, *Nature structural & molecular biology*, **2012**, 19, 253-259.
45. R. Thomsen, M.H. Christensen, *Journal of medicinal chemistry*, **2006**, 49, 3315-3321.
46. S.F. Le Grice, F. Gruninger-Leitch, *European journal of biochemistry / FEBS*, **1990**, 187, 307-314.
47. K. Das, J.D. Bauman, A.D. Clark, Jr., Y.V. Frenkel, P.J. Lewi, A.J. Shatkin, S.H. Hughes, E. Arnold, *Proceedings of the National Academy of Sciences of the United States of America*, **2008**, 105, 1466-1471.
48. A.M. Wensing, V. Calvez, H.F. Gunthard, V.A. Johnson, R. Paredes, D. Pillay, R.W. Shafer, D.D. Richman, *Topics in antiviral medicine*, **2015**, 23, 132-141.
49. B.C. Johnson, G.T. Pauly, G. Rai, D. Patel, J.D. Bauman, H.L. Baker, K. Das, J.P. Schneider, D.J. Maloney, E. Arnold, C.J. Thomas, S.H. Hughes, *Retrovirology*, **2012**, 9, 99.
50. WHO, 18th WHO Model List of Essential Medicines, in: W.H. Organization (Ed.), WHO, 2013.
51. C. Katlama, S.G. Deeks, B. Autran, J. Martinez-Picado, J. van Lunzen, C. Rouzioux, M. Miller, S. Vella, J.E. Schmitz, J. Ahlers, D.D. Richman, R.P. Sekaly, *Lancet*, **2013**, 381, 2109-2117.
52. M. Kaul, G.A. Garden, S.A. Lipton, *Nature*, **2001**, 410, 988-994.
53. K. Robertson, J. Liner, R.B. Meeker, *J Neurovirol*, **2012**, 18, 388-399.
54. L. Waters, M. Fisher, A. Winston, C. Higgs, W. Hadley, L. Garvey, S. Mandalia, N. Perry, M. Nicola, M. Nelson, *Aids*, **2011**, 25, 65-71.
55. A. Nguyen, S. Rossi, D. Croteau, B.M. Best, D. Clifford, A.C. Collier, B. Gelman, C. Marra, J. McArthur, J.A. McCutchan, S. Morgello, D. Simpson, R.J. Ellis, I. Grant, E. Capparelli, S. Letendre, C. Group, *The Journal of antimicrobial chemotherapy*, **2013**, 68, 1161-1168.
56. A. Herath, N.D.P. Cosford, *Beilstein Journal of Organic Chemistry*, **2017**, 13, 239-246.